Synthesis and Integration of Nanoparticles in Thin Film Nanocomposite Membranes for Water Treatment

by

Zayed Almansoori

A thesis submitted in partial fulfillment of the requirements for the degree of

Master of Science

Department of Mechanical Engineering

University of Alberta

Abstract

The most widely used method for desalination, the process of removing salts and minerals from saltwater for human consumption and irrigation, is membrane technology. There are various types of membrane technologies, but the use of thin film nanocomposite (TFN) polyamide (PA) membranes for nanofiltration (NF) and reverse osmosis (RO) are central to seawater and wastewater treatment. TFN membranes incorporate nanoparticles (NPs) into their PA layer which are able to increase the membranes contaminant rejection, mechanical strength, and water flux, resulting in a more efficient separation process that produces water with higher quality. This thesis focuses on the synthesis and integration of conductive indium tin oxide (ITO) NPs into membranes with the goal of demonstrating improved thermal stability and hydrophilicity.

The NPs are dispersed in the organic solution during synthesis of the TFN membrane, however the tendency of NPs to form large aggregates has been a major limitation to their successful integration. The challenge of aggregation extends to widespread applications of NPs, where utilizing monodisperse and stable suspension of NPs is essential. The aggregation of NPs becomes more challenging when there is less affinity between the dispersed phase (NPs) and the continuous phase (solvent), such as, dispersion of hydrophilic metal oxide NPs into a nonpolar (organic) solvent. The objective of the first part of this study is to systematically investigate the synergistic effects of eight dispersion parameters on the size an d stability of indium tin oxide (ITO) NPs in heptane. The matrix of experimentation was designed using an L_{18} Taguchi method. The analysis of variance (ANOVA) of the experimental results revealed that the most significant factors on the size and stability of NPs were the mass of ITO NPs and the volume of

the dispersing agent. Taguchi signal-to-noise (SN) ratio analysis was used to determine the optimal factor levels for the preparation of well-dispersed and stable NP suspensions. Confirmation tests were carried out at the suggested levels of the ANOVA predictive model, and highly stable ITO NPs in heptane with the size distribution of 43.0–68.3 nm were obtained. The results of the parametric study can be used for a broad range of applications where effective stabilization of metal oxide NPs in organic solvents is desired.

The ITO NP suspension is utilized in the second part of the work to synthesize ITO TFN membranes. The presence of ITO NPs at a weight percentage of 0.02% were shown to nearly double the water flux of the control membrane during the treatment of salt water, from 25.3 LMH to 41.5 LMH, while maintaining a 98% rejection of salt. Contact angle measurements showed an increase in the concentration of ITO NPs in the PA layer successfully increased the hydrophilicity of the membrane. The incorporation of ITO NPs was shown to increase the zeta potential of the PA layer across a wide range of pH measurements. Thermogravimetric analysis demonstrated that the ITO TFN membrane demonstrated greater thermal stability, with a thermal degradation temperature of 472°C compared to a temperature of 455°C, than the control membrane. Finally, field emission scanning electron microscopy, transmission electron microscopy, and an energy-dispersive X-ray spectroscopy acquisition system were used to show well integration of the ITO NPs in the PA layer without the formation of defects.

Preface

The contents of Chapter 2 were published in the journal of Ultrasonics Sonochemistry on September 6, 2017, under the title "Parametric study on the stabilization of metal oxide nanoparticles in organic solvents: A case study with indium tin oxide (ITO) and heptane". I was responsible for data collection, analysis, as well as the manuscript composition. B. Khorshidi and B. Sadri were involved in the initial brainstorming, training, and editing of the work. M. Sadrzadeh was the supervisory author. The DOI and full citation is shown below:

Z. Almansoori, B. Khorshidi, B. Sadri, and M. Sadrzadeh, "Parametric study on the stabilization of metal oxide nanoparticles in organic solvents: A case study with indium tin oxide (ITO) and heptane," *Ultrason. Sonochem.*, vol. 40, no. September 2017, pp. 1003–1013, 2017.

https://doi.org/10.1016/j.ultsonch.2017.09.012

A combination of the contents of chapter 2 and 3 were orally presented at the 3rd International Conference on Desalination Using Membrane Technology in Gran Canaria, Spain. The presentation was titled "Parametric study on the stability of indium tin oxide nanoparticles in organic solvent as a prerequisite for synthesizing defect-free thin film nanocomposite membranes". A link to the Oral Programme is copied below:

https://www.elsevier.com/__data/assets/pdf_file/0005/274757/MDES2017_Oral-Programme_8-March.pdf

Finally, the results of my thesis work were presented at the 2017 University of Alberta 3MT (Three Minute Thesis) competition and I received second place. The presentation was posted online and can be found with the following url:

https://youtu.be/T1nwoMla8Ew

Acknowledgements

I never thought I would publish a paper on the topic of nanoparticles. I wasn't even sure I would continue education after I finished my bachelors degree, but sometimes life has a funny way of working out.

I first met Mohtada in my third year of Undergrad; he was one of the professors I got along best with. I ran into him randomly during my last semester of fourth year and, after chatting, he offered me a position to do a Masters. I am grateful for the support he has given me these past two years and I am happy I ran into him in that hallway. I'd also like to thank the coauthors of my paper Behhnam Khorshidi and Sadri. My colleagues in our research group were wonderful, and I could not have finished my degree without them. I owe a big thank you to each one of you.

I'd also like to take this opportunity thank my friends, family, and everyone I have met during my time at the University of Alberta. Edmonton became a home to me and I have all of you to thank for that.

Table of Contents

Chapter 1: Introduction ---------- 1

1.1 The importance of water and a chance for equality---------- 1

1.2 The use of Membrane Technology in Water Treatment ---------- 2

1.2.1. Modifying the membrane synthesis procedure ---------- 4

1.2.2. Chemical grafting of functionalized materials to the surface ---------- 5

1.2.3. Development of mixed matrix membranes by incorporation of nanofillers ---------- 6

1.3 Literature Review: The use of metal oxides for the synthesis of TFN membranes ---- 6

1.4. Driving force and equations related to membrane separation and fouling ---------- 8

1.5 Challenge of aggregation: An introduction to the importance for use in the fabrication of membranes and a literature review ---------- 10

1.6 Thesis structure ---------- 13

1.7 Thesis contribution ---------- 14

Chapter 2: Parametric study on the stabilization of metal oxide nanoparticles in organic solvents: A case study with indium tin oxide (ITO) and heptane---------- 15

2.1. Introduction ---------- 16

2.2. Materials and methods ---------- 18

2.2.1. Materials ---------- 18

2.2.2. Synthesis of ITO NPs ---------- 18

2.2.3. Experimental methodology ---------- 19

2.2.4. Preparation of ITO suspension ---------- 21

2.2.5. Evaluation of the size, stability and chemical composition of the ITO NPs ---------- 22

2.3. Results and discussions ---------- 23

2.3.1. Initials size and stability of ITO NPs in heptane ---- 23

2.3.2. Statistical analysis ---- 24

2.3.3. Trend of influence of the dispersion parameters ---- 26

a) Mean effect of the mass of ITO NPs in heptane ---- 26

b) Average influence of the amount of dispersing agent in the suspension ---- 27

c) Mean effect of the volume of organic solvent ---- 29

d) Effect of immersion depth of the sonication probe ---- 30

e) Intensity and duration of sonication ---- 31

f) Effect of the temperature of the sonication bath ---- 33

g) Effect of length of shaking of the NPs suspension ---- 34

2.3.4 Optimal setting of the control factors and confirmation experiments ---- 34

2.4. Conclusion ---- 37

Chapter 3. The incorporation on Indium Tin Oxide onto the surface of the membrane to create Thin Film Nanocomposite membranes ---- 38

3.1 Introduction ---- 38

3.2 Materials and Methods ---- 40

3.2.1 Materials ---- 40

3.2.2 Synthesis of TFC and TFN membrane ---- 40

3.2.3 RO filtration flux measurement and rejection ---- 41

3.2.4 FO filtration flux measurement and rejection ---- 43

3.2.5 Other Characterization Techniques ---- 44

a) Microscopy Techniques ---- 44

b) Elemental analysis ---- 44

c) Contact Angle ---- 44

d) Zeta Potential ---- 45

e) Thermal Stability Analysis ---- 45

3.3 Results and Discussion----------45
3.3.1 Membrane morphology ----------45
3.3.2 Contact Angle ----------48
3.3.3 Flux and rejection performance in RO and FO ----------50
3.3.4 Zeta potential ----------52
3.3.5 TGA analysis ----------54
3.4 Conclusion----------55
Chapter 4. Conclusion and future work ----------56
4.1 Conclusion----------56
4.2 Future work----------58
4.3 Contributions ----------61
References ----------62

List of Tables

Table 2.1: List of control variables and their corresponding levels used in the L18 table. ------20

Table 2.2: Matrix of experiment based on L18 OA design.----------21

Table 2.3: Results of ANOVA test for the size of ITO NPs in heptane. ----------24

Table 2.4: Results of ANOVA test for the stability of ITO NPs in heptane. ----------25

Table 4.1: Composition of SW ----------59

List of Figures

Figure 1.1: The IP reaction between two monomers to generate the PA layer in TFC membranes ---------- 4

Figure 1.2: RO and FO process diagrams. In RO, pressure is applied to a feed solution higher than the osmotic pressure, water molecules are then passed through the membrane and collected in the permeate chamber. In FO, the draw solution with low water chemical potential is separated from the high chemical feed solution and water molecules from the feed are transported to the draw solution. ---------- 9

Figure 1.3: FESEM images of the ITO TFN membrane surface showing: (a) a low size cluster of ITO NPs. (b) a poor distribution of NPs across the membrane ---------- 13

Figure 2.1: Schematic synthesis route of ITO NPs ---------- 19

Figure 2.2: Initial particle size and stability of the ITO NPs in heptane. ---------- 23

Figure 2.3: Effect of the mass of ITO on mean responses and SN ratios for (a) particle size and (b) stability. ---------- 27

Figure 2.4: Effect of volume of surfactant on mean responses and SN ratios for (a) particle size and (b) stability ---------- 28

Figure 2.5: Effect of volume of heptane on mean responses and SN ratios for (a) particle size and (b) stability. ---------- 29

Figure 2.6: Effect of immersion depth of the sonication probe on the mean responses and SN ratios for (a) particle size and (b) stability. ---------- 31

Figure 2.7: Effect of (a,b) sonication energy and (c,d) duration of sonication on mean responses and SN ratios for particle size and stability. ---------- 32

Figure 2.8: Effect of the temperature of the sonication bath on the (a) particle size and (b) stability and their corresponding SN ratios. ---------- 33

Figure 2.9: Effect of duration of shaking on mean responses and SN ratios for (a) particle size and (b) stability. ---------- 34

Figure 2.10: Optimized experimental results for particle size based on the plot of SN ratios. ---- 35

Figure 2.11: (a) FESEM image of the solid ITO NPs, (b) EDX elemental composition of the synthesized ITO NPs, (c) TEM image of ITO NPs dispersion for the optimal confirmation test, (d) initial particle size distribution of the ITO NPs obtained by DLS for the optimal confirmation test. ---------- 36

Figure 3.1: The formation of the PA layer atop a microporous support to form a TFC membrane. (a) is a cross-sectional FESEM image and (b) is the chemical reaction to form the PA layer where monomer 1 is MPD and monomer 2 is TMC.----------40

Figure 3.2: Schematic view of cross-flow RO pressure-driven filtration setup ----------42

Figure 3.3: Schematic view of cross-flow FO concentration-driven filtration setup ----------43

Figure 3.4: TEM cross-sectional images of the different membranes. (a) is the base TFC membrane, (b) is the 0.01% ITO TFN 1 membrane, (c) is the 0.02% ITO TFN 2 membrane. (1) is with a magnification of 22,000 , (2) is with a magnification of 56,000. The dashed line indicates the separation between the PES sublayer and the PA layer, the entirety of (2b) and (2c) is a magnification of the PA layer.----------46

Figure 3.5: FESEM images of the (a) base TFC membrane (b) TFN 1 and (C) TFN 2 at a magnification of 10,000 ----------47

Figure 3.6: SEM+EDX images of the base (a) TFC, (b) TFN 1, and (C) TFN 2.The tables in images 1a-2c show the atomic (at) % and weight (wt) % of each element. Images (1a-c) are at a magnification of 500x and the EDX is of the entire image. Images (2a-c) are at a magnification of 5,000x and EDX is only of a specific region highlighted by the orange circle. Images (3a-c) are the accompanying elemental distribution plots. ----------48

Figure 3.7: Increasing the weight% of ITO resulted in a decrease in contact angle at each level ----------49

Figure 3.8: RO pure water flux results showing an improved flux with the addition of ITO -----50

Figure 3.9: RO saline flux and rejection results showing the addition of ITO results in an improvement in flux without sacrificing selectivity----------51

Figure 3.10: FO water and saline flux results showing another improvement for water flux with a small change in saline flux----------52

Figure 3.11: Zeta potential measurements showing a more positive shift in the pH zeta potential curve due to the presence of ITO ----------53

Figure 3.12: Weight loss of ITO TFN membrane as a function of temperature showing increased thermal stability of the ITO TFN membrane compared to the base TFC. ----------54

Chapter 1. Introduction

1.1 The Importance of water and a chance for equality

Access to drinking water and sanitation is accepted as a basic human right [1]. In fact, the majority of the 17 UN sustainable development goals can be strongly linked to the importance of equal and affordable access to water [2]. Even with this knowledge, there are unfortunately still over 700 million people who do not have access to clean water and over 40% of the global population is affected by water scarcity [3]. On top of its vital importance to human health, the lack of clean water leads to millions dying from diseases that are associated with inadequate water supply, hygiene, and sanitation [3]. While Canada is home to one-fifth of the world's freshwater, according to the World Wildlife Foundation, there are still issues surrounding water supply and sustainability [4]. One such industry is the Alberta oil sands, which uses an average of 3 barrels of river water for each barrel of oil produced [5]. This water must also be stored in tailings ponds after use, due to high concentrations of organic acids and solids leeched from the bitumen during extraction, resulting in a zero discharge policy for the used water [5]. Membrane separation technology has appeared as one of the methods to treat this volatile water, however, there are still inefficiencies that must be overcome [5].

By the year 2025, there are expected to be 29 countries who experience water scarcity [6]. In the Middle East, this challenge is being tackled by desalination; nations like Saudi Arabia, Kuwait, and Qatar are dependent on desalination for the majority of their water needs [6]. In my home country of the United Arab Emirates, which has the second highest desalination usage globally, it is reported that seawater desalination requires ten times more energy than surface fresh water production [7]. In fact, in 2015 it was estimated that over 300 million people globally rely on freshwater from desalination [8]. The most popular method for turning seawater and wastewater into clean drinking water is also through membrane separation technology, using a combination of nanofiltration and reverse osmosis [9]. This requires applying high hydraulic pressure to drive water across a membrane to reject contaminants. An advantage membrane technology has over other methods, such as distillation, is that it requires a lower energy input since the separation occurs without the need for a phase transition [10]. However, there is still a cost barrier that is preventing membrane technology from being more accessible.

1.2 The Use of membrane technology in water treatment

There are two different types of driving force for membranes that are evaluated in this thesis, pressure driven by a pump, and osmotic pressure through a concentration gradient. There are four different grades/classifications of the membrane for the pressure-driven processes, microfiltration (MF), ultrafiltration (UF), nanofiltration (NF), and reverse osmosis (RO), occasionally referred to as hyperfiltration [11,12]. These classifications are based on their pore size or their molecular weight cutoff, a way to measure which particles will pass through a membrane, based on their molecular weight and measured in Daltons [11,12]. MF has a pore size range of 0.1-10 μm and can remove over 99% of all particles/turbidity found in water, as well as 99.99% of all bacteria and protozoa, and is usually operated at a pressure in the range of 30-500 kPa. UF has a pore size range of 0.01-0.1 μm and can, in addition, remove viruses and remove some suspended solids such as proteins, UF is usually run at 30-500 kPa as well. NF has a pore size range from 1-10 nm, and removes over 95% of all viruses and over 95% of suspended solids, NF has a typical operating pressure of 500-1000kPa. Finally, RO has a molecular weight cutoff of 100-200 Daltons and is capable of removing most solids including metal ions and dissolved salts; it is operated at an operating pressure between 1000-5000 kPa.

In MF and UF membranes, the pore size is the significant parameter for determining what molecules pass. For NF and RO, the most important parameter of the transport is based on the chemical properties, and ultimately the solution-diffusion mechanism, of the membrane. The transfer of the molecules begins with molecules being absorbed onto the surface of the membrane and then desorbed at the permeate side after diffusing across the membrane [13]. The difference between RO and NF membranes is that the structural network in NF membranes is more open, reducing its ability to reject/retain monovalent salts such as Na^+ or Cl^-. The high operating pressure results in RO and NF technology for seawater becoming too costly and energy intensive for widespread use [9,14].

Forward Osmosis (FO) has emerged as a reliable alternative for seawater desalination. Instead of being driven by hydraulic pressure applied across the membrane, FO generates osmotic pressure based on a concentration difference between two solutions, the draw and feed [9,14]. As a result of this chemical potential difference, water molecules are drawn from the feed side to the draw. Due to the nature of its driving force, FO is an alternative low energy intensive type of desalination.

One of the key challenges in membrane separation is the issue of fouling[15]. Fouling consists of a buildup of contaminates attaching onto the membranes surface or inside the pores of the membrane [15]. A consequence of fouling is the reduced performance of a membrane during filtration [15]. Membrane fouling can be divided into four categories, (1) inorganic fouling, also known as scaling, (2) colloidal fouling, (3) biological fouling, and (4) organic fouling. All four types of fouling occur during seawater desalination [16]. There is a high degree of fouling and biofouling from oil and dissolved solids for membranes used for treating water in the oil sands industry and this is one of the key challenges hindering membrane technology becoming a more efficient technology for this industry [5]. Membrane fouling is more severe with hydrophobic membranes than hydrophilic ones as a result of hydrophobic interactions between the membrane surface and hydrophobic solutes and microbial cells in water [15,17]. As a result, it is more desirable to synthesize more hydrophilic membranes. This can be achieved by the incorporation of multifunctional polymers (chemical grafting) or nanomaterials (synthesis of hybrid or mixed matrix membranes) to the surface and bulk of membranes.

There are several ways membranes can be classified. One such classification is symmetric versus asymmetric. Symmetric membranes have the same density across the thickness of the membrane. Asymmetric membranes, on the other hand, have a denser layer at the top, generally referred to as a skin layer and a more porous sublayer. One of the most important fields of research in membrane technology is surface modification of this skin layer to improve overall membrane performance [15]. The membranes fabricated in this thesis are asymmetric thin film composite (TFC) membranes that are prepared via interfacial polymerization (IP). TFC membranes typically contain:

1. A non-porous selective top layer which improves the selectivity/rejection of the membrane.
2. A porous bottom layer which adds mechanical stability to the membrane.

The top layer forms by the IP reaction, which is a reaction between m-phenylenediamine (MPD) monomers in water and trimesoyl chloride (TMC) monomers in an organic solvent, the reaction at the interface between these two monomers results in a nonporous polyamide (PA) layer forming on the surface of the membrane. For the formation of the PA layer, a previous protocol established in our research group was followed, as shown in Figure 1.1 [18]. This process is discussed in more detail in chapter 3. The reaction between TMC and MPD may result

in two possible structures, a crosslinked portion (denoted as *m* in the top right of Figure 1.) and a linear moiety (denoted as *n* in the top right of Figure 1.) [19]. The crosslinking density (*m*/*m*+*n*) can be adjusted by controlling various parameters during IP reaction, including reaction temperature, type and concentration of monomers and additives, and curing procedure.

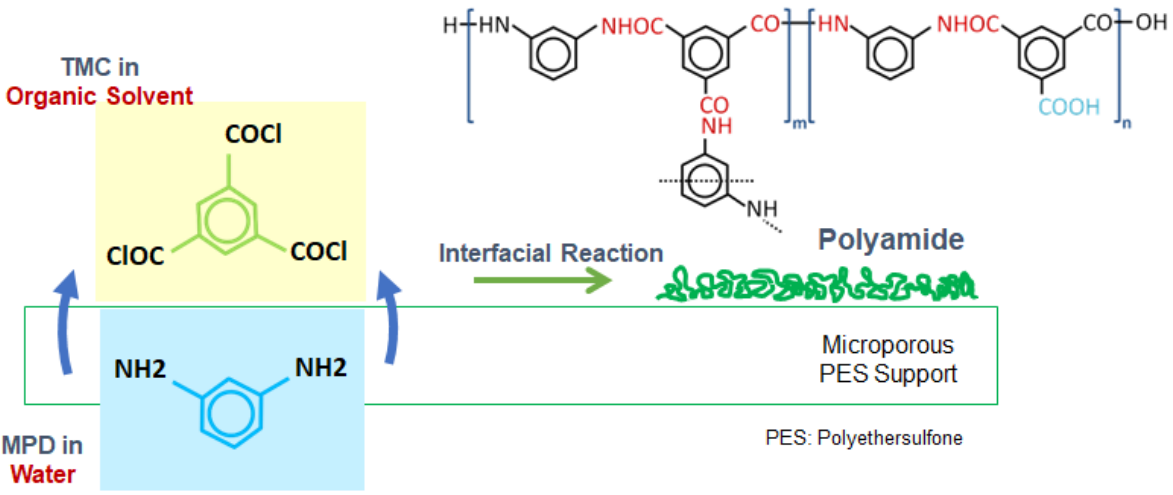

Figure 1.1: The IP reaction between two monomers to generate the PA layer in TFC membranes

The selective PA layer in the TFC membrane plays the primary role in water filtration. TFC membranes, along with cellulose acetate membranes, are the most popular types of RO membranes. In comparison to cellulose acetate membranes, TFC membranes exhibits superior water flux, pressure compaction resistance, organic matter rejection, and salt rejection, and a broader range of operating temperature and pH [19]. The PA layer has the advantage of good thermal stability, being able to withstand temperatures up to 50 °C, a reasonable chemical stability, as well as a wide operating pH from 3 to 11 [12]. Since the invention of TFC membranes, numerous efforts have been devoted to modification of these membranes in terms of water permeation, contaminant rejection and antifouling properties. Some of these efforts are presented here.

1.2.1. Modifying the membrane synthesis procedure

The membrane synthesis procedure can be modified by optimizing the interfacial polymerization reaction for the formation of the active PA layer. The properties of this thin PA

layer (thickness, roughness, and crosslinking density) strongly depend on the type and concentration of monomers and additives, reaction time and temperature, and post-treatment techniques.

There are several parameters which influence the quality of the PA layer and thus the performance of the TFC membrane. These parameters include polymerization reaction and temperature, curing temperature, monomer concentration, and type and concentration of various additives. The effect of these parameters on the PA layer is complex and there is no clear consensus on their trend of influence [20]. For example, it was suggested by Liu et al. that increasing the polymerization reaction time between the two monomers results in a decrease in flux [21]. However, in another study by Khorshidi et al. increasing the reaction time to 60s from 15s between the two monomers results in an insignificant change in the flux and rejection of the membrane, suggesting that the reaction time is near instantaneous [20].

Another factor that influences the performance and morphology of the PA layer is the monomer concentration [20]. It is first necessary to understand that the PA layer forms in two general stages, as opposed to a gradual linear increase. In the first stage, at the interface between the water and organic solution a fast reaction between MPD and TMC molecules occurs, forming an ultrathin (incipient) PA film atop the surface of the PES film. The MPD then diffuses towards the organic solution, resulting in a slower growth of a secondary polymerized layer with a ridge-and-valley structure. An increase in the weight concentration of MPD in the aqueous solvent results in a membrane with high salt rejection and low flux, as well as a thicker PA layer. The higher thickness of PA layer can be attributed to an increase in the available MPD molecules in the reaction zone. The opposite is true for an increase in the weight concentration of TMC in the organic solvent; the result is a membrane with low salt rejection and higher flux, but a thinner PA layer. This can be attributed to the TMC molecules contributing to a denser PA layer, hindering MPD molecules from diffusing to the organic phase.

1.2.2. Chemical grafting of functionalized materials to the surface

Most of recent studies have been conducted on applying surface modification techniques, e.g., chemical grafting of functional materials and hydrophilic polymers to the membrane surface [22–25]. The main goal was to increase the hydrophilicity of the membrane and make them more negatively charged. In spite of the fact that chemical grafting can induce

the desired properties to the membrane, the functional materials can be easily washed away during long-term operation by cross-flow filtration. Also, the grafting method cannot be easily scaled up and the applied chemicals are not usually environmentally friendly [22].

1.2.3. Development of mixed matrix membranes by incorporation of nanofillers

TFC membranes can be further improved by incorporating nanomaterials into the PA layer which is the focus of this study. This is accomplished by dispersing the nanomaterials in the organic solution, and the resulting membrane is known as a thin film nanocomposite membrane (TFN). However, the addition of nanomaterials to a polymer film, for the fabrication of a robust hybrid membrane, is more complicated than it appears. If nanomaterials are not handled properly, they may not induce the desired functionality to the polymer and even may deteriorate its separation properties. The major challenge to this is the severe aggregation of the nanomaterials and their pore distribution and dispersion within the polymer matrix. For TFN membranes, the nanomaterial aggregates cannot be accommodated in a thin PA layer (100-300 nm thickness), which makes the aggregation effect even more severe. The non-homogeneous dispersion of nanomaterials within the polymer forms non-selective voids at the interface of the polymer and inorganic nanomaterials and thus reduces the rejection of contaminants.

For the synthesis of TFN membranes, It is better to disperse the nanomaterials in the organic phase as opposed to the aqueous phase, as a large amount of nanomaterials would be removed during the removal of excess aqueous solution during IP [26]. The performance of TFN membranes is affected by numerous factors including size, hydrophilicity, charge, and dispersion quality of the nanomaterials, as well as the ratio of nanomaterials within the membrane polymer matrix [27].

1.3 Literature review: The Use of metal oxides for the synthesis of TFN membranes

The performance a membrane is typically evaluated based on permeation properties, fouling tendency, and thermal/chemical resilience. The ideal membrane for desalination and water treatment application should provide high water flux (recovery), high contaminant rejection (water quality), antifouling property, and reasonable mechanical properties that ensures the membrane for long-term operation.

One method to improve the above-mentioned properties of the membranes is to incorporate NPs onto the surface [26,28,29]. These nanoparticles have the ability to induce desirable properties into the nanocomposite membrane due to their small size [29–31]. Some of the most commonly used metal oxide NPs include titania, alumina, zirconia, magnetite, and silica [28]. According to the literature, the incorporation of NPs polymer matrix may improve the water permeation, but at the expense of sacrificing separation properties. In other words, the addition of larger size and poorly dispersed NPs cannot overcome the typical trade-off relation between flux and rejection in membranes [18].

The first mention of TFN membranes was a study done by Jeong et al. in 2007 [32]. The study showed that the addition of NaA zeolite nanoparticles in the PA layer was able to almost double water flux without sacrificing rejection. The authors hypothesized that the high solute rejection and enhanced water permeation was due to the steric and Gibbs-Donnan exclusion. The Gibbs-Donnan exclusion results in a charged membrane surface due to a difference in the electrical and chemical potential between the feed solution and the permeate solution. Steric exclusion is due to larger sized solutes in water which are unable to occupy the same space and thus cannot approach the hydrophilic membranes surface. Silica NPs (MCM-41) were used by Yin et al. for TFN membranes and once again showed an increase in water flux, to 46.6 LMH from 28.5 LMH without the sacrifice in the rejection of NaCl and Na_2SO_4 [33]. In addition to showing well-embedded particles in the PA layer and their influence on the surface zeta potential, the authors discussed that the likely mechanism for the improved water flux was both reduced crosslinking in the PA layer as well as shorter pathways for water flow through the hydrophilic porous and ordered MCM-41 structure. Titanium Oxide nanoparticles were used by Rajaeian et al. who improved flux by the addition of the metal oxide in both the aqueous solution and the organic TMC solution [34]. The membranes synthesized in this study showed a low NaCl rejection of less than 60% and a further decrease by the addition of more titanium oxide in the membrane. This was evidenced by a decrease of rejection of NaCl from 45% to 35%, as a result of increasing the weight percentage of titanium oxide to 0.1% from 0.05% This result was attributed to larger pore sizes in the PA layer due to a disturbance by the NPs in the reaction between the chloride and amine monomers.

In addition to improving flux, the addition of NPs has been shown to add desirable characteristics to the membrane. Nguyen et al. showed that the addition of a layer of silver and

titanium dioxide NPs improved the antibacterial properties of a membrane 11 times against adenosine triphosphate [35]. The FO membranes were prepared by first immersing the membrane in silver nitrate and irradiated with UV lamps for 20 minutes, followed by immersion in water containing 0.5 wt% poly (sodium styrene sulphonate) for 40 hours, and finally immersed in a titanium oxide solution for two hours. The titanium oxide NPs were able to decompose the organic matter, thus preventing silver nanoparticles from being covered and diminishing their antibacterial effect. There is some debate over the mechanism that silver NPs kill bacteria [35]. Yu et al., similarly, showed that the addition of silver and titanium dioxide NPs improved the antibacterial properties of the thin PA layer [36]. The authors hypothesized that the silver NPs release small amounts of silver ions, which are able to induce cell death. This mechanism is highly dependent on the size of silver nanoparticles. In addition to antibacterial properties, other desirable properties have been added to the membrane as a result of NP incorporation. As an example, both alumina and silica nanoparticles have been shown to improve the mechanical stability of the membrane [37].

The use of metal oxides for the composition of inorganic membranes is growing in popularity [15]. The incorporation of single-element oxide nanoparticles can improve hydrophilicity, mechanical strength, thermal stability, permeate flux, selectivity, and surface charge of the nanocomposite membrane [15,34,36]. One metal oxide that has yet to be incorporated into TFN membranes is indium tin oxide (ITO), which is widely used in the production of LEDs, solar cells, and optoelectronic devices. This is despite a study conducted by Khorshidi et al. which shows that the inclusion of ITO inside the polymer matrix of a membrane, prepared via phase inversion, was able to improve the conductivity and flux of the membrane without a loss in the separation efficiency [38]. One barrier to the use of metal oxides lies in the challenge of proper dispersion in the organic solvent. This challenge will be addressed in chapter 2, and the fabrication and testing of ITO TFN membranes will be shown in chapter 3.

1.4. Driving force and equations related to membrane separation and fouling

A membrane can be described as a selective barrier that allows the passage of certain molecules but rejects the passage of others. A simplified process diagram of both RO and FO are shown in Figure 1.2. In Figures 1.2a and 1.2b, the RO process is shown which uses hydraulic pressure to push water through a semipermeable membrane. In Figure 1.2c and 1.2d due to the

difference in water chemical potential, water is permeated from the feed solution to the draw solution.

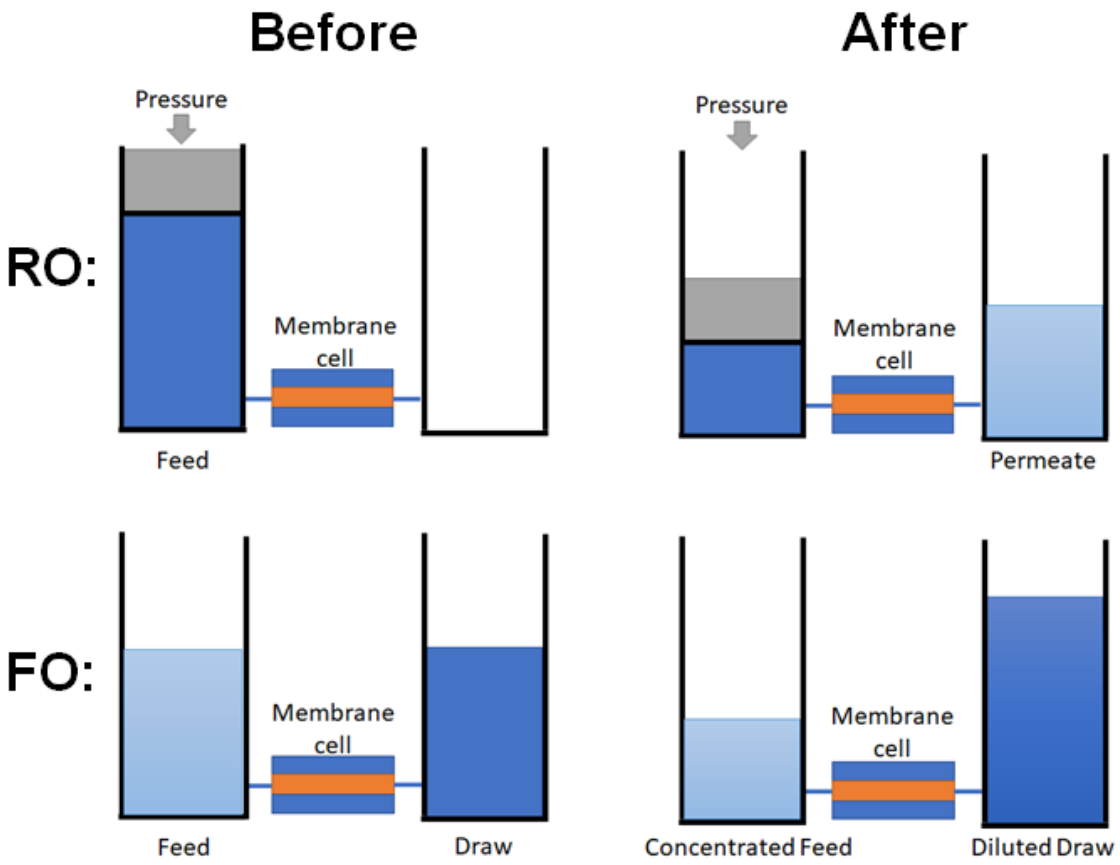

Figure 1.2: RO and FO process diagrams. In RO, pressure is applied to a feed solution higher than the osmotic pressure, water molecules are then passed through the membrane and collected in the permeate chamber. In FO, the draw solution with low water chemical potential is separated from the high chemical feed solution and water molecules from the feed are transported to the draw solution.

In pressure driven processes, the water flux can be calculated using the following formula:

$$J_W = A(\Delta P - \Delta\pi) \tag{1.1}$$

here J_w is the water flux across the membrane, with units L/m^{2}h, A is the membrane permeability coefficient (it is also reciprocal to the resistance of flow), ΔP is the applied pressure, and $\Delta\pi$ is the osmotic pressure of the feed solution. Equation 1 assumes an ideal case that there is no solute

(salt) permeation through the membrane. In reality, however, there is no perfect membrane since there is always a slight permeability of the membrane towards the solutes. A more accurate equation adds a coefficient σ, the membranes reflection coefficient towards that solute, in front of the osmotic pressure:

$$J_W = A(\Delta P - \sigma\Delta\pi) \tag{1.2}$$

In FO there is an absence of applied pressure and the driving force is the difference in the osmotic pressure of the two solutions, caused by a concentration difference. The flux can be obtained as follows:

$$J_W = A\Delta\pi = A(\pi_D - \pi_F) \tag{1.3}$$

where π_D is the osmotic pressure of concentrated draw solution, and π_F is the osmotic pressure of the lower concentrated feed solution.

Furthermore, the rejection of the membrane for both RO and FO can be found by measuring the concentration in both the permeate and the feed. For example, if the membrane is being tested for salt rejection then the following equation would be used to measure rejection:

$$R = (1 - \frac{C_p}{C_f}) \times 100 \tag{1.4}$$

here R is the salt rejection, C_p is the concentration of salt in the permeate, and C_f is the concentration of salt in the feed.

1.5 Challenge of aggregation: An introduction to the importance for use in the fabrication of membranes and a literature review

One of the key challenges to utilizing NPs and importing their desired functionality is to prevent them from aggregating (forming clusters) and keeping the particles in the nanoscale [30,39–41]. Strong attraction forces are what cause the NPs to aggregate. For a variety of applications, a low particle size can be considered as the most important feature in practical application [15,42,43]. Another used term for aggregation is agglomeration. The terms are often used interchangeably, though a generally defined difference is that, agglomeration refers to weaker/loosely bonded particles and aggregation refers to strongly bonded particles.

Aggregation can be attributed to surface interactions including van der Waals interactions [15,44]. Fundamentally, the aggregation of particles occurs in two steps [41]:

1. The particles must collide. This is primarily achieved by Brownian diffusion, however it can also be the result of sedimentation or the motion of the fluid that the particles are suspended in. For particles that are less than about 100 nm in size, Brownian diffusion is typically the driving force that causes the collisions between particles[44].
2. The interactions of the particles colliding must allow for permanent contact. If the particles simply repel each other after colliding, aggregation will not occur.

For the manufacturing of NPs, there are two categories of aggregation: homo-aggregation, or aggregation of two similar particles, and hetero-aggregation, which is of dissimilar particles[44]. In classic Derjaguin-Landau-Verwey-Overbreak (DLVO) theory, attachment is determined by the sum of attractive and repulsive forces. However classical DLVO alone is not sufficient for an accurate prediction of aggregation, additional forces have been added to better match results on the experimentation of NP aggregates. The collection of these forces is known as the extended DLVO forces (XDLVO). Van der Waals forces originate from the interactions of the electrons in the particles and calculates the net attraction, V, in the following way:

$$\frac{V_{vdw}}{kT} = \frac{-A}{6kT}\left(\frac{2a^2}{s(4a+s)^2} + \frac{2a^2}{(2a+s)^2} + \ln\frac{s(4a+s)^2}{(2a+s)^2}\right) \tag{1.5}$$

where, a is the average particle radius, A is the Hamaker Constant, k is the Boltzmann constant, T is the absolute temperature, and s is the distance between the interacting surfaces. The electrostatic double layer originates from the attraction/repulsion of charged surfaces and is calculated using the following equations:

$$\frac{V_{EDL}}{kT} = \frac{64\pi mkT(a+\delta)^2}{\kappa(s+2a)}[\tanh(\frac{ze\psi_d}{4kT})]^2 \exp^{-\kappa(s-2\delta)} \tag{1.6}$$

where $\kappa = [\frac{\sum_i^N e^2 z_i^2 n_i}{\varepsilon_r \varepsilon_0 kT}]^{1/2}$,which is the inverse of the Debye screening length, or the thickness of the diffuse electric double layer. In these formulas, δ is the stern layer thickness, z is the electrolyte valence, Ψ_d is the diffuse potential (approximately the zeta potential), ε_r is the relative static permittivity, and ε_0 is the vacuum permittivity.

The electrostatic double layer and van der Waals attraction make up the classical DLVO theory. The additional forces in XDLVO are (1) magnetic attraction, which originates from the electron spin, (2) hydrophobic forces (Lewis acid-base) which is due to the entropy associated

with separating hydrogen bonds in water, (3) osmotic repulsion due to the concentration difference of ions between two particles, (4) elastic-steric repulsion which is due to the resistant loss of entropy of molecules on the particles surface due to compaction, and (5) bridging attraction where surface molecules form bridges to other particles.

The aggregation/agglomeration of the NPs is one of the main problems in the fabrication of TFN membranes [26]. The aggregation of NP not only reduces their active surface area, limiting the impact of their desirable qualities, it can also create defects, or holes, in the PA structure [26]. Another issue during fabrication is the difficulty in dispersing hydrophilic nanoparticles in the organic phase, a challenge that arises from the NPs tendency to aggregate in non-polar solvents [26]. Though increasing the weight percentage of NPs in the PA layer will result in a higher potential for imparting desirable qualities, an increase in the concentration of NPs increases their susceptibility to aggregate [44].

The challenge previous researchers at our lab faced with using in lab synthesized indium tin oxide (ITO) to fabricate TFN membranes was the aggregation of the NPs resulting in defects and inconsistencies across the membrane. ITO was synthesized using indium chloride, tin chloride, and ammonium hydroxide; a more in-depth protocol is presented in chapter 2. Field emission scanning electron microscopy was used to take images of the surface of the TFN membranes which used these NPs. The images are shown in Figure 1. which show a high aggregation of NPs and an inconsistent surface. As shown in Figure 1.3a, the NPs themselves carried a low size of less than 50nm but were still prone to aggregation and forming nanoclusters.

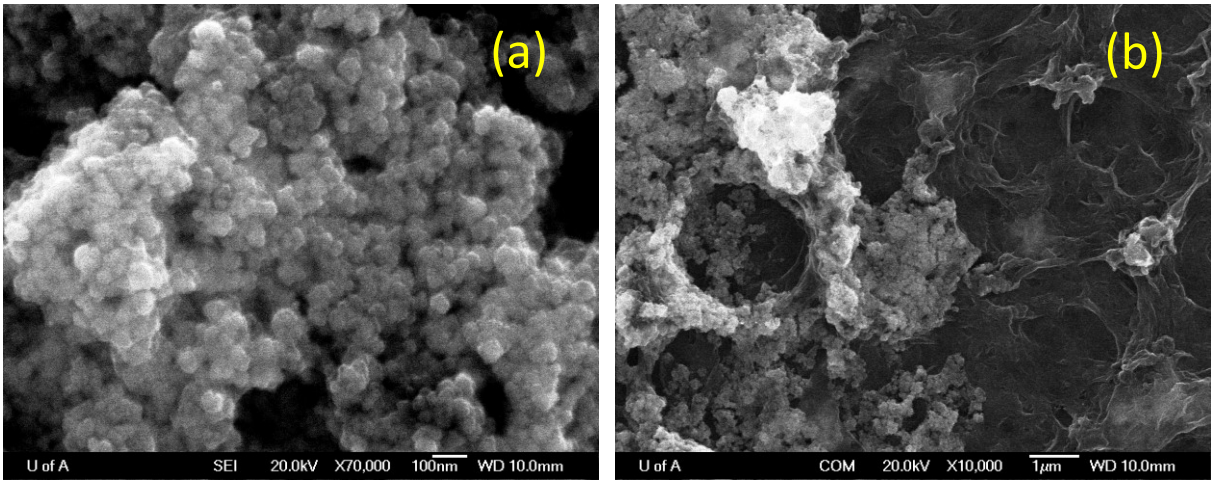

Figure 1.3: FESEM images of the ITO TFN membrane surface showing: (a) a low size cluster of ITO NPs. (b) a poor distribution of NPs across the membrane

The presence of these clusters highlights the need for a study to better improve the dispersion of the NPs in the non-polar organic solvent. This includes a comprehensive study of the parameters associated with the dispersion and to identify an optimal particle loading for the fabrication of high-performance TFN membranes.

1.6 Thesis structure

This thesis is organized in a paper-based format. Chapter 2 is based on a published journal article and focuses on the optimization of the synthesis process of ITO NPs. This chapter takes a Design of Experiments approach (DOE) to study the different parameters in the dispersion process of ITO NPs in heptane. The goal of this chapter was to create a small-size stable dispersion of ITO in heptane that overcomes the challenge of aggregation and is ready for use in fabricating TFN membranes.

Chapter 3 is based on a paper that is being prepared for submission and shows the improved performance of the TFN membranes with ITO incorporated onto the PA layer. Flux measurements for pure water flux, as well as saline water flux and rejection are conducted for both RO and FO processes. In addition to a saline water flux and rejection measurement for RO, the membranes are also characterized for contact angle, zeta potential, and thermal gravimetric analysis, and imaged using field emission scanning electron microscopy, energy-dispersive X-ray spectroscopy acquisition system, and transmission electron microscopy.

Finally, chapter 4 is a summary of the main outcomes of the thesis and contains a concluding statement. The section ends with recommendations for future work related to the study and a summary of published works/achievements made with the work.

1.7 Thesis contributions

A barrier to the fabrication of high-performance ITO TFN membranes is the aggregation of the ITO NPs in the organic solvent. To reduce aggregation of NPs and improve dispersion, an understanding of the different parameters associated with dispersion of the ITO NPs was studied in chapter 2; which resulted in stable low size ITO NPs. In addition, the outcome of this work can serve as a guideline to be used for better dispersing other NPs in the future. In chapter 3 the addition of ITO was shown to improve the water flux of the TFC membrane to nearly double without a sacrifice in rejection. The incorporation of ITO was shown to make the membrane more hydrophilic, thus increasing water permeability, and change the zeta potential; while also having a good dispersion inside the polyamide layer.

Chapter 2. Parametric study on the stabilization of metal oxide nanoparticles in organic solvents: A case study with indium tin oxide (ITO) and heptane

The contents of this chapter were published in the journal of Ultrasonics Sonochemistry on September 6 2017 under the same title. Behnam Sadri helped with training, the initial planning stage of the project, and preliminary experiments. Behnam Khorshidi helped with analysis and provided guidance for the literature review. The DOI and full citation is shown below:

Z. Almansoori, B. Khorshidi, B. Sadri, and M. Sadrzadeh, "Parametric study on the stabilization of metal oxide nanoparticles in organic solvents: A case study with indium tin oxide (ITO) and heptane," *Ultrason. Sonochem.*, vol. 40, no. September 2017, pp. 1003–1013, 2017.

https://doi.org/10.1016/j.ultsonch.2017.09.012

2.1. Introduction

The emergence of nanoparticles (NPs) have made a substantial contribution to the improvement of technologies across multiple disciplines [45–47]. The incorporation of NPs into conventional materials with the aim of developing advanced nanocomposites has led to considerably enhanced properties such as heat resistance, permeability, mechanical strength, and electrical conductivity in a variety of applications [48–50]. The magnitude of the induced properties to the resulting nanocomposites is mainly influenced by the size and the surface properties of the NPs [29,31]. The smaller size of NPs provides a higher ratio of surface area to volume, which enables NPs with tuned surface functionalities to govern the behavior of the host materials [51,52].

It is widely accepted that a major challenge to utilize the desired functionality of NPs is to preserve them in the nanoscale by hindering their agglomeration and/or aggregation [30,39–41]. In a variety of applications where monodisperse and stable suspensions of the NPs are required, the aggregation of the NPs is the key limitation which negatively impacts the quality of the final product [42,43]. One of the widely used methods for breaking down the large NP structures is via sonication [53–55]. Sonication involves the use of sound energy to create acoustic cavitation that involves formation, growth, and implosion of tiny bubbles [53,56]. There are two main types of sonication, namely direct and indirect sonication. Direct sonication is the process of immersing a sonication probe into a liquid suspension to transfer the energy via ultrasonic waves. Direct sonication delivers high energy intensity to the NPs system and is, therefore, most effective for dispersing dry powders and for the initial dispersion of nanomaterials [57]. Indirect sonication is the process of propagating ultrasonic waves through a liquid bath, with the NPs suspension is inside a container and placed in the bath. This technique is often used to resuspend particles which have been already processed using direct sonication. It has been reported that an initial increase in the intensity and duration of sonication decreases particle size and improves stability. However, prolonged ultrasonication leads to the re-agglomeration of NPs [54,55]. Recent evidence showed that the nanofluid characteristics such as viscosity, interfacial tension, and energy density are influential parameters on the efficiency of deagglomeration during sonication [58,59]. The suspension viscosity and energy density can be affected by altering the amount of NPs and the volume of solvent used to prepare the NPs suspension [53].

A recent study on the direct sonication of vermiculite particles showed that increasing the temperature of the suspension leads to a reduction in particle size [60]. However, a high sonication temperature can result in evaporation of the solvent and thus a change in the composition of NPs suspension. Therefore, it is important to monitor the temperature of the bath during sonication [53]. Furthermore, the contact length of the sonication probe [53] and frequent shaking of the NP suspension [61] have been reported to be influential on the transferred energy to the suspension and as a result, the size and dispersion of NPs. Finally, utilizing surfactants as dispersing agents (also known as capping agents) has been proved to be one of the most effective ways to increase the stability of NPs in suspensions [62–65]. Depending on the type and concentration, dispersing agents will modify the surface properties of the NPs and prevent their aggregation by promoting steric stabilization and overcoming the inherent van der Waals forces between them in either aqueous or nonaqueous solvents [30,66–69]. Regarding that, low molecular weight surfactants such as oleic acid, myristic acid, and octadecylamine are commonly used due to their high adsorption to the NPs surface [70–73].

Although a great deal of research has been carried out using both direct and indirect sonication, there are still no versatile protocols for preparing NP dispersion, making it necessary to test the effects of different sonication parameters for a particular system of NP and solvent to determine the optimal sonication conditions [55,67,74]. Hence, the objective of the present work is to systematically study the synergistic effect of the several dispersion parameters on the size and stability of indium tin oxide (ITO) NPs and find the optimal setting for their effective dispersion in an organic solvent (heptane). The dispersion of metal oxides in heptane, as a nonpolar solvent, presents a challenge due to low dielectric constant of heptane, as well as, low solubility of metal oxides in low-polarity solvents [75]. Overcoming this challenge is highly of interest in applications such as fabrication of nanocomposite membranes via interfacial polymerization reaction where an organic solvent is used in the fabrication process [18]. ITO is one of the most widely used transparent electrode materials in a variety of applications including solar cells, light-emitting diodes and devices, optoelectronic devices, liquid crystal displays, and laser diodes [76,77]. The main advantages of ITO NPs are that they have low resistivity, high transparency, high carrier concentration, high mobility, as well as ease of processing [73,76]. Also, ITO has been shown to improve the thermoelectrical characteristics and antifouling properties of phase inversion polymeric membranes for water treatment applications [38]. The

dispersion parameters in this study include (i) the immersion depth of the sonication probe, (ii) the volume of the heptane, (iii) the temperature of the sonication bath, (iv) the intensity of sonication, (v) the duration of sonication, (vi) the length of shaking of the NPs suspension, (vii) the mass of ITO NPs, and (viii) the volume of the dispersing agent. These parameters were studied at different levels using a robust design of experiment (DOE) method known as Taguchi. Three basic principles of design of experiments (randomization, replication, and blocking) were applied, and the response variables (size and stability of ITO NPs) were evaluated by the Analysis of Variance (ANOVA), Taguchi marginal graphs, and signal-to-noise ratio analyses.

2.2. Materials and methods

2.2.1. Materials

Indium chloride, tin chloride ($InCl_3$ and $SnCl_4$ from Strem Chemicals Inc., Newburyport, MA, USA), and ammonium hydroxide (NH_4OH, Sigma-Aldrich) were used for the synthesis of ITO NPs. Proprietary BYK-106 (Altana AG, Wallingford, USA), alkylolammonium salts of the lower molecular weight polycarboxylic acid polymer [78], was used as a dispersing agent to prepare nano-dispersed suspensions of ITO NPs in heptane (Sigma-Aldrich).

2.2.2. Synthesis of ITO NPs

The procedure of synthesizing ITO NPs is presented in Figure 2.1. The first step is a reaction between indium chloride and tin chloride (with 10/1 molar ratio of In/Sn) in water in the presence of ammonium hydroxide. The product of this reaction is a mixture of tin oxide-indium hydroxide and ammonium chloride. In the next step, this mixture is centrifuged and washed with water several times to remove the ammonium chloride. The resulting white compound of tin oxide-indium hydroxide is then crystallized at 700° to remove water and generate yellow ITO crystals. These yellow crystals are finally hydrogenated with a gas stream 10% H_2 and 90% Ar in a tube furnace at 350°C to produce blue conductive ITO crystals. Positive sites are formed in some areas due to the reaction of oxygen atoms on the ITO crystals with hydrogen atoms to generate H_2O. The amount of indium chloride and tin chloride in the reaction, the temperature of both the crystallization and hydrogenation stages, and the H_2 and Ar gas flow rates, all affect the properties of the synthesized NPs.

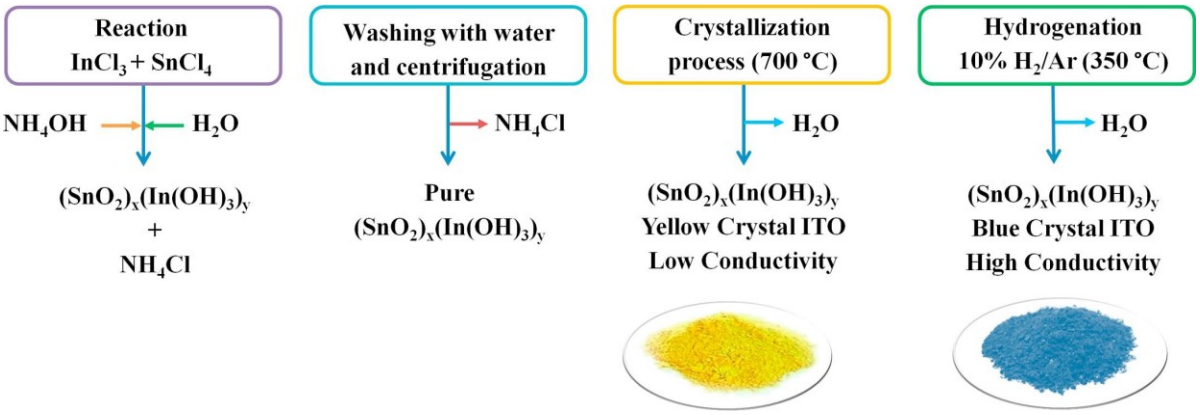

Figure 2.1: Schematic synthesis route of ITO NPs

2.2.3. Experimental methodology

The systematic study on the dispersion of ITO NPs in heptane was carried out using a robust design of experiment called Taguchi. This method, as a highly fractional factorial design, is mainly used to find the best combination of controllable factors to make the results less sensitive to the changes in uncontrollable (noise) factors [79].

Eight control factors were considered as influential parameters on the size and stability of NPs based on preliminary screening experiments. The control factors were then designed using Taguchi L_{18} standard orthogonal array (OA) [20,80]. Table 2.1 presents the list of control factors in this study and their corresponding levels of variation. The L_{18} OA was generated and the results were analyzed using the Statistica software. The L_{18} design allows testing of one factor at two levels, and seven factors at three levels, by conducting 18 experiments as illustrated in Table 2.2.

Table 2.1: List of control variables and their corresponding levels used in the L18 table.

(Symbol) Control factor	Levels		
	I	II	III
(A) Immersion depth of probe (cm)	0.75	1.5	-
(B) Volume of heptane (ml)	25	30	35
(C) Temperature of water bath (°C)	11.0	18.5	21.5
(D) Intensity of sonication (kJ)	8.4	48	70
(E) Duration of sonication (min)	90	120	150
(F) Duration of shaking (min)	0	1	2
(G) Mass of ITO NPs (g)	0.3	0.6	0.9
(H) Volume of BYK (µl)	50	100	150

Three basic principles of DOE namely randomization, replication, and blocking were applied in this study. Randomization of the order of the experiments was carried out to limit the introduction of bias into the system. Experiments were replicated twice to provide an estimate of experimental error. Blocking was done by using ITO NPs all from the same synthesis batch to improve precision and reduce the variability of the results [81]. Furthermore, Analysis of Variance (ANOVA) with a confidence level of 95% was used to determine statistically significant variables.

Table 2.2: Matrix of experiment based on L18 OA design.

Experiment	Factor level							
	A	B	C	D	E	F	G	H
1	1	1	1	1	1	1	1	1
2	1	1	2	2	2	2	2	2
3	1	1	3	3	3	3	3	3
4	1	2	1	1	2	2	3	3
5	1	2	2	2	3	3	1	1
6	1	2	3	3	1	1	2	2
7	1	3	1	2	1	3	2	3
8	1	3	2	3	2	1	3	1
9	1	3	3	1	3	2	1	2
10	2	1	1	3	3	2	2	1
11	2	1	2	1	1	3	3	2
12	2	1	3	2	2	1	1	3
13	2	2	1	2	3	1	3	2
14	2	2	2	3	1	2	1	3
15	2	2	3	1	2	3	2	1
16	2	3	1	3	2	3	1	2
17	2	3	2	1	3	1	2	3
18	2	3	3	2	1	2	3	1

2.2.4. Preparation of ITO suspension

Based on the matrix of experimentation in Table 2.2, particular amounts of ITO NPs, solvent, and BYK-106 were first mixed. Next, the suspension was placed in a water bath and cooled to approximately 15.3°C to prevent overheating and evaporation of the heptane during sonication. The suspension was then sonicated for 90 to 150 minutes using a probe sonicator (Qsonica CL-334 equipped with titanium alloy probe) with an output frequency of 20 kHz and a power of 4-39 W. The duration of pulse ON was 30 minutes and the duration of pulse OFF was 4 minutes. Direct sonication was conducted in pulsed mode, as opposed to continuous mode to minimize the undesired temperature gain and evaporation of solvent [55,74]. To control the

temperature, the water in the bath was replaced after each interval, and then the suspension was shaken manually for a particular period (based on the table of experimentation) to improve mixing. After the final sonication step, the suspension was shaken by hand once more for 15 seconds. Finally, 1.0 ml of the sample was drawn from the middle of the suspension and diluted ten times for size measurement using dynamic light scattering (DLS) machine.

2.2.5. Evaluation of the size, stability and chemical composition of the ITO NPs

The size of ITO NPs was measured using a DLS instrument (ALV/CGS-3 compact goniometer, ALV-GmbH, Langen, Germany). The detection angle and the laser wavelength were adjusted at 632.80 nm and 90°, respectively. The viscosity and refractive index of the solvent (heptane) were set to 0.386 and 1.388, respectively, for the DLS analysis.

The initial recording from the DLS was used to compare the initial size of the NPs. Moreover, the DLS measurement was continued for 34 minutes with constant time intervals to evaluate the stability of the NPs over time. The measurements were taken every two minutes for the first eight minutes, and every five minutes after that. A stability parameter was defined in this study to evaluate the aggregation rate of the NPs as:

$$\text{Stability Parameter} = \frac{R_{in}}{t} \times \left(\frac{R_{max} - R_{min}}{R_{min}} \right) \tag{2.1}$$

where R_{in} is the initial hydrodynamic radius measured by the DLS, t is the measurement time period (34 minutes in the present study), and R_{max} and R_{min} are the maximum and minimum recorded radiuses, respectively. Equation (1) is basically similar to the reported studies in the literature which express the aggregation kinetics as the initial rate of increase in hydrodynamic radius of the suspended particle with time [82,83]. However, it represents the aggregation phenomenon more precisely by taking the sedimentation of NPs into account. In this equation, the term R_{in} serves as a scaling factor which allows comparing the results of different experiments with different size ranges. The term $\left(\frac{R_{max} - R_{min}}{R_{min}} \right)$ shows the rate of aggregation and sedimentation relative to the size of NPs in the dispersion. The unit of the stability parameter is [m/s] which allows the parameter to be considered as a measure of precipitation velocity of aggregated NPs. Hence, the smaller the stability parameter, the more stable the NPs suspension. Furthermore, field emission scanning electron microscopy (FESEM, Zeiss Sigma 300 VP) and

transmission electron microscopy (TEM, Philips/FEI Morgagni 268, The Netherlands) was used to observe the shape of the ITO NPs. The elemental analysis was conducted using an energy-dispersive X-ray spectroscopy acquisition system (EDX, Bruker). The zeta potential of the ITO suspension at the optimum condition was measured using Malvern Zetasizer Nano ZSP (Worcestershire, UK).

2.3. Results and discussions

2.3.1. Initials size and stability of ITO NPs in heptane

Figure 2.2 illustrates the initial size and stability parameter of the ITO NPs which were prepared based on designed matrix of experimentation (Table 2.2). The initial hydrodynamic radius varied from 66 nm to 2737 nm, and the stability parameter ranged from 0.2 m/s to 157.9 m/s. The significant change of results for the different combinations of factors demonstrates the remarkable effect of factors on the size and stability of NPs. This is more evident when comparing the smallest size and most stable NPs in run 3 with the largest and least stable ones in run 8, as illustrated in Figure 2.2. The unstable and large size of NPs in run 8 can be attributed to the low amount of surfactant and high amount of ITO and heptane.

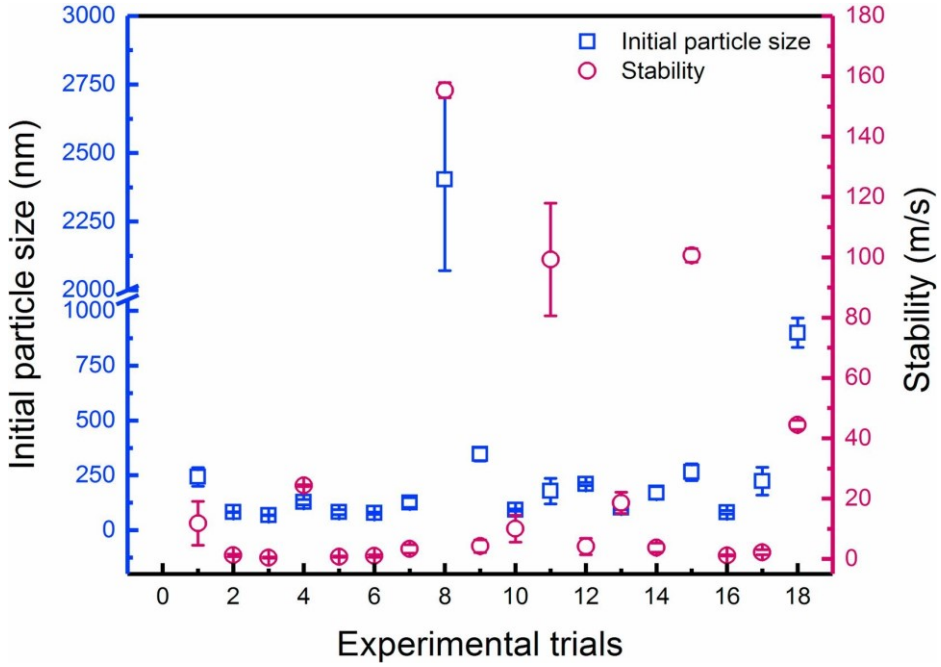

Figure 2.2: Initial particle size and stability of the ITO NPs in heptane.

2.3.2. Statistical analysis

Tables 2.3 and 2.4 present the results of ANOVA test based on the size and stability of the ITO NPs in heptane. Using a 95% confidence level, a recorded p-value lower than 0.05 (larger F-values) indicates that the control factor has a significant influence on the results. The sum of squares value in Tables 2.3 and 2.4, is an expression showing the total variation of results that can be attributed to each factor. The degree of freedom for each factor is one less than the number of levels for that factor. Mean square is the sum of squares divided by the degree of freedom [84,85]. The F value in the tables is calculated by the ratio of factor variance over error (residual) variance as:

$$F = \frac{\text{Mean Square}_{\text{factor}}}{\text{Mean Squar}_{\text{residual}}} \tag{2.2}$$

Table 2.3: Results of ANOVA test for the size of ITO NPs in heptane.

(Symbol) Control factor	ANOVA - Particle size				
	Sum of squares	Degrees of freedom	Mean square	F	p
(A) Immersion depth of probe	4.30	1	4.30	0.36	0.554216
(B) Volume of heptane	602	2	301	25.3	0.000003
(C) Temperature of water bath	204	2	102	8.55	0.002072
(D) Intensity of sonication	56.6	2	28.3	2.38	0.118200
(E) Duration of sonication	160	2	80.0	6.75	0.005735
(F) Duration of shaking	256	2	128	10.75	0.000675
(G) Mass of ITO NPs	244	2	122	10.27	0.000852
(H) Volume of BYK	484	2	242	20.36	0.000015
Residual	238	20	11.9	---	---

Table 2.4: Results of ANOVA test for the stability of ITO NPs in heptane.

(Symbol) Control factor	ANOVA – Stability				
	Sum of squares	Degrees of freedom	Mean square	F	p
(A) Immersion depth of probe	792.0	1	792.0	8.665	0.008046
(B) Volume of heptane	115.0	2	57.54	0.629	0.543240
(C) Temperature of water bath	57.81	2	28.90	0.316	0.732583
(D) Intensity of sonication	1224	2	612.0	6.696	0.005941
(E) Duration of sonication	1035	2	517. 5	5.660	0.011267
(F) Duration of shaking	127.5	2	63.75	0.696	0.509795
(G) Mass of ITO NPs	2238	2	1119	12.23	0.000339
(H) Volume of BYK	1721	2	860.5	9.410	0.001317
Residual	1829	20	91.45	---	---

Using the degree of freedom of factors and the residual, a minimum *F* value to indicate that a factor is significant can be extracted from the F-distributions tables [86]. In this study, the extracted F-statistics from the F-distribution table is 4.88 for a 95% confidence level. Based on the F-values and p-values in Tables 2.3 and 2.4, the factors significant in influencing particle size, in the order of significance were identified as follows: (i) the volume of heptane, (ii) the volume of BYK, (iii) the duration of shaking, (iv) the mass of ITO, (v) the temperature of water bath, and (vi) the duration of sonication. The ANOVA test revealed that the immersion depth of the sonication probe, as well as the intensity of sonication, did not have a significant influence on the size of the ITO NPs.

Regarding the influential factors on the stability of the NPs, the ANOVA results revealed that the mass of ITO NPs had the largest influence on the stability of the final suspension in heptane. The other significant factors were identified as, in the order of significance, (ii) the volume of BYK, (iii) the immersion depth of the sonication probe, (iv) the intensity and (v) the duration of sonication. It is worth noting that the volume of heptane which had the most

significant influence on the size of ITO NPs was insignificant on their stability. A similar trend was realized for the effect of the temperature of the water bath which was insignificant on the stability but was found to influence the size of NPs, significantly. Furthermore, changing the intensity of sonication was found to alter only the stability of the NPs but not their size distribution.

2.3.3. Trend of influence of the dispersion parameters

Employing the Taguchi method for designing the matrix of experimentation allows identification of the the mean trend of influence of the dispersion parameters via marginal mean plots, also known as the 'main effects' plot. A marginal mean plot illustrates the response for each factor level, while the level settings of the other factors are also changing concurrently. The plot can thus be used to understand the average trend of influence of each control factor regardless of the variation of the other factors. The plots of marginal means for both particle size and stability are presented in Figures 2.3-2.9. The SN ratio in these figures represents a statistical parameter called signal-to-noise (SN) ratio [87,88]. In a robust experiment, the results are desired to only change by the experimenter's signals (controllable factors) and should not be affected by noise factors which are either unknown or uncontrollable [89,90]. Hence the primary goal of using the Taguchi method is to maximize the SN ratio. Higher values of SN ratio identify settings of control factor that minimize the effect of noise factors. The applied equation for the calculation of SN ratio depends on the goal of an experiment. Three standard SN ratios are related to larger-is-better (e.g., strength or yield) smaller-is-better (e.g., contamination or impurity) and nominal-is-best (e.g., dimensions). In the present study, the main objective is to minimize both the particle size and stability parameter. Hence, smaller-the-better SN ratio is chosen which can be calculated as follows [88,91]:

$$\mathrm{SN} = -10\log\left(\frac{1}{n}\sum_{i=1}^{n} Y_i^2\right)$$

Here n is the number of experiments and Y is the response variable.

a) Mean effect of the mass of ITO NPs in heptane

The average influence of the mass of ITO NPs on the initial size and stability of the NPs along with their corresponding SN ratio are presented in Figure 2.3. Based on the mean plot in

Figure 2.3a, increasing the mass of the ITO NPs from 0.3 g to 0.6 g resulted in smaller size NPs. A likely explanation is that the presence of more particles in the suspension increased the frequency of collisions among NPs and consequently enhanced the chance of breakage of aggregates [53,92]. However, the addition of more ITO NPs to heptane, up to 0.9 g, increased the size of NPs. It could be due to an increase in the viscosity and the acoustic conductivity of the suspension which dampened the cavitation pressure and thus led to an increase in the required power to achieve smaller size NPs [53]. The plot of the stability parameter of the ITO NPs (Figure 2.3b) shows that by increasing the loading of NPs in the suspension the stability of NP suspension decreased which implies a faster aggregation rate of NPs. This result can also be attributed to the effect of NPs concentration on the viscosity and acoustic conductivity of NPs suspension [53,92].

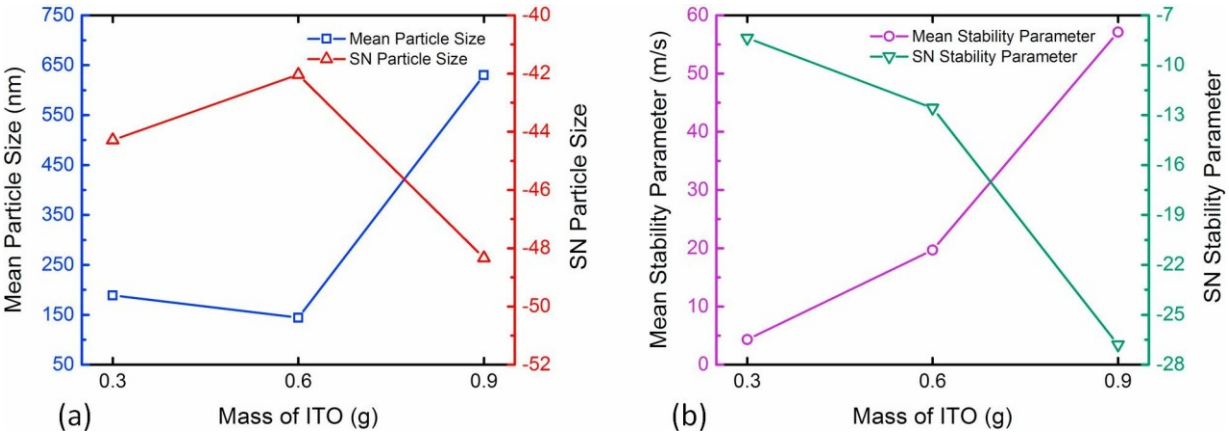

Figure 2.3: Effect of the mass of ITO on mean responses and SN ratios for (a) particle size and (b) stability.

b) Average influence of the amount of dispersing agent in the suspension

The effect of BYK as a dispersing agent on the size and stability of the ITO NPs is illustrated in Figure 2.4. BYK, which is basically a surfactant, lowers the aggregation of NPs by reducing their surface free energy and tuning their surface chemistry by incorporating desired functional materials to their surface [93,94]. Based on the DLVO theory, the stability of NPs suspensions is governed by the balance of two main forces: repulsive electrostatic interaction and attractive van der Waals force [95]. To obtain a stable NPs suspension, the repulsive forces among NPs must be strong enough to prevent irreversible aggregation due to the attractive

forces. Since the electrostatic repulsive forces of ITO NPs is weak, it is essential to use surfactant molecules on their surfaces to screen the van der Waals interactions [96,97]. Selecting a suitable dispersing agent depends on the type of the dispersion medium, chemical structure of surfactant, and the binding strength of the surfactant headgroups to the surface of NPs [98]. For the dispersion of NPs in nonpolar organic solvents, as in this study, effective stabilizers should possess both functional anchor groups and long-chain hydrophobic stabilizing moieties (tail groups) [99]. The unanchored or weakly anchored stabilizing moieties may flocculate and induce an adverse effect on the stability of NPs.

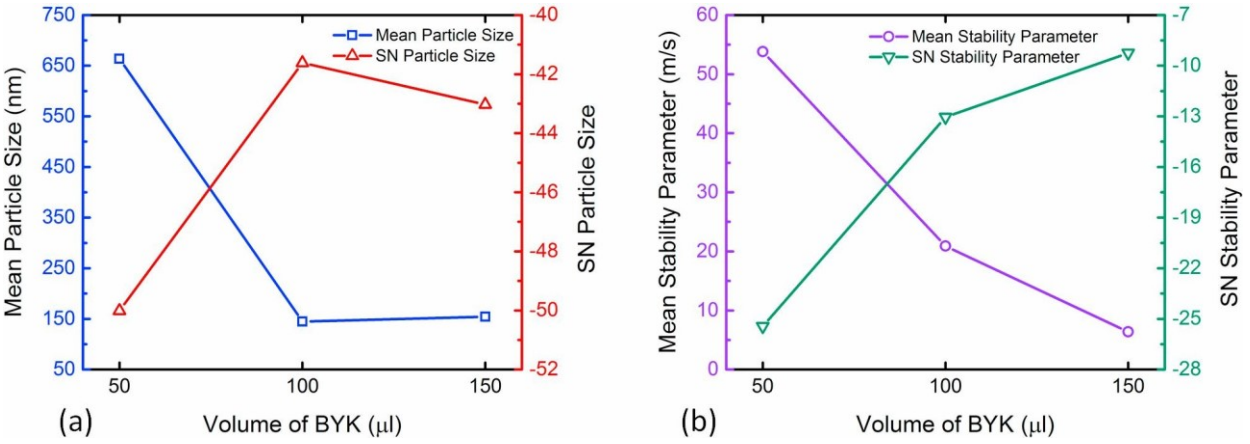

Figure 2.4: Effect of volume of surfactant on mean responses and SN ratios for (a) particle size and (b) stability

Based on the results in Figure 2.4, an increase in the amount of BYK in heptane from 50 µl to 100 µl decreased the size of the dispersed NPs, significantly. This result indicates that surfactant molecules are predominately attached to the ITO NPs and improved their dispersion within the organic solution [66]. It can also be concluded that, after the addition of 100 µl BYK, its stabilizing moieties were still soluble in heptane and its head groups were effectively anchored to the surface of ITO NPs. However, the incorporation of more BYK into heptane solution from 100 nm to 150 nm had a minimal effect on the final size of the NPs, implying the presence of extra BYK in the solution. Regarding the stability of the ITO NPs, Figure 2.4b demonstrates that increasing the concentration of BYK in heptane significantly lowered the aggregation rate and improved the stability of resulting NPs suspension. It is worth noting that, although the presence of more dispersing agent molecules is beneficial for preparing a stable suspension of the NPs, the final concentration of the dispersing agent may be constrained by the

desired physicochemical properties of the NPs suspension such as the interfacial tension, viscosity, and solubility.

c) Mean effect of the volume of organic solvent

In addition to the amount of the dispersed NPs and dispersing agent, the volume of the carrying medium can also play a major role by altering the energy density within the solution. The energy density expresses the amount of delivered energy per unit volume of carrying medium (J/ml). At the same intensity of the sonication power and the concentration of NPs, a larger energy density results in greater disruptive effects within the suspension [53]. As can be observed in Figure 2.5a, an increase in the volume of heptane from 25 ml to 30 ml slightly decreased mean particle size from 145.7 to 137.4 nm, and a further increase from 30 to 35 ml resulted in a substantial increase in the NPs size from 137.4 to 680 nm. This observation can be attributed to the low energy density within the heptane which was not enough for the separation and dispersion of the NPs from their initially aggregated structure. It has been reported that a sufficiently high energy density can break all secondary aggregates (2–100 μm) into primary aggregates (0.03–1 μm), while even very high energy density might not be able to break primary aggregates down into single nanoparticles [100]. In contrast to the effect on the particle size, the variation of the volume of heptane did not have a significant influence on the stability of the ITO NPs as shown in Figure 2.5b and ANOVA analysis in Table 2.4.

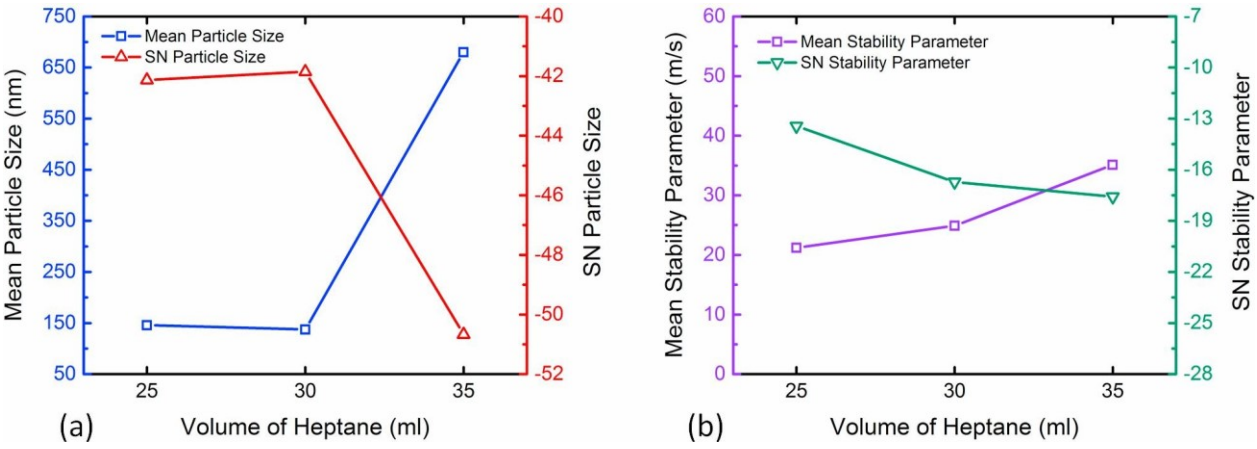

Figure 2.5: Effect of volume of heptane on mean responses and SN ratios for (a) particle size and (b) stability.

d) Effect of immersion depth of the sonication probe

Figure 2.6 shows the effect of immersion depth of the sonication probe on the size and stability of the ITO NPs in the heptane. Proper selection of the immersion depth is necessary to improve the dissipation of the acoustic energy and thus improves the fluid circulation and to prevent foaming and evaporation of the solvent. The dissipation of the acoustic energy in a given medium can be estimated as [53]:

$$I_x = I_0 e^{-2\alpha x}$$

where I_x is the acoustic intensity at a distance x from the source, I_0 is the acoustic intensity at the source (power/area), and α is the absorption coefficient which is directly proportional to the dynamic viscosity of the carrying liquid (μ, kg/ms), as well as the acoustic frequency (f, 1/s), and inversely related to the liquid density (ρ, kg/m^3) ($\alpha \propto 2\mu f^2/3\rho$).Based on Equation 4, the immersion depth represents the distance from the energy source and directly affects the intensity of acoustic energy received by the NPs. It is well know that the dissipation of the acoustic energy generates the acoustic streaming which is defined as the circulation of a steady flow near the vibrating elements. Increasing the sonication power was reported to increase the fluid velocity, significantly [101–104]. Also, the liquid circulation velocity was found to be dominant in the zones closer to the source of energy (sonication probe) and is substantially lower at the walls and the bottom of container [101]. Hence, increasing the water depth or decreasing the immersion depth was reported to lower the average velocity [103].

The increased velocity of the fluid by increasing the immersion depth slightly decreased the size of NPs, as shown in Figure 2.6. This observation is in agreement with the ANOVA results in Table 2.3 that implied an insignificant change in the particle size due to a change in the height of the sonication probe. A possible explanation for the diminished effect of immersion depth can be a higher collision rate of the NPs when there is more contact area between the probe and the suspended NPs. This enhances the chance of aggregation of NPs due to short range intermolecular interactions like van der Waals forces. This counter effect has influenced the stability results as shown in Figure 2.6b. As can be observed, increasing the immersion depth of the sonication probe from 7.5 mm to 15 mm lowered the stability of the NP suspension and increased the rate of aggregation of the NPs.

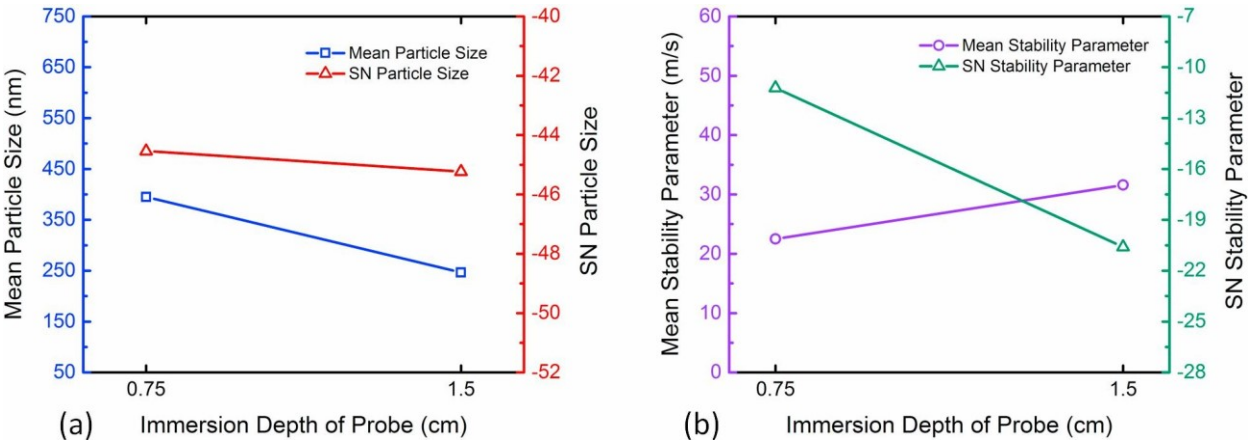

Figure 2.6: Effect of immersion depth of the sonication probe on the mean responses and SN ratios for (a) particle size and (b) stability.

e) Intensity and duration of sonication

In order to improve the dispersion of the NPs in a liquid medium, it is highly needed to optimize the amount of delivered disruptive energy to the suspension which is related to the applied power and the duration of sonication ($E = P \times t$) [74]. An insufficient amount of sonication energy cannot break the aggregated structures, while a prolonged sonication may lead to re-agglomeration of the dispersed NPs [55]. Figures 2.7a and 2.7b illustrate the effect of sonication energy on the size and stability of the ITO NPs in heptane. As can be seen, an increase in the sonication energy from 8.4 kJ to 48 kJ has notably improved the stability of the NPs while it slightly affected the size of dispersed NPs. This behavior can be justified considering the cavitation cycle during the sonication.

High-intensity ultrasonic waves generate transient cavitation and acoustic streaming (fluid flow due to acoustic pressure gradient) which are effective parameters for stirring the NP suspension [56,105]. Acoustic cavitation results in formation, growth, and collapsing of micro bubbles under cyclic high-intensity ultrasonic waves (expanding and collapsing during negative and positive pressure cycles, respectively) [56]. In fact, the NPs oscillate at their mean position; bubbles are generated at the interparticle spaces and when these bubbles collapse they will release energy to the suspension and disrupt the aggregates [106]. On the other hand, it has been reported that the sonication at very high vibration amplitudes, in the pulse mode, generates large bubbles for which the time between cavitation cycles (formation, growth, and implosion of bubbles) is not sufficient to collapse them and reduces cluster breakage [54,106]. Such a trade-

off relationship shows that increasing the intensity of ultrasonication does not necessarily reduce the size of NPs. As can be observed in Figure 2.7, a further increase in the sonication energy from 48 kJ to 70 kJ adversely affected the size and stability of the NPs. It was found that increasing the sonication energy from 48 kJ to 70 kJ resulted in larger NPs with higher aggregation rates.

Similar to the intensity of sonication, the duration of sonication also affects the supplied energy to the NPs suspension and thus alters the size and stability of NPs. Figures 2.7c and 2.7d demonstrate that there is an optimal time period for providing the sonication energy to the suspension. It was found that by increasing the time of sonication from 1.5 to 2 hr, a suspension with a larger particle size of NPs and lower stability was prepared. However, extending the duration of sonication from 2 to 2.5 hr decreased the size of the NPs, significantly, and improved the stability of the NPs suspension.

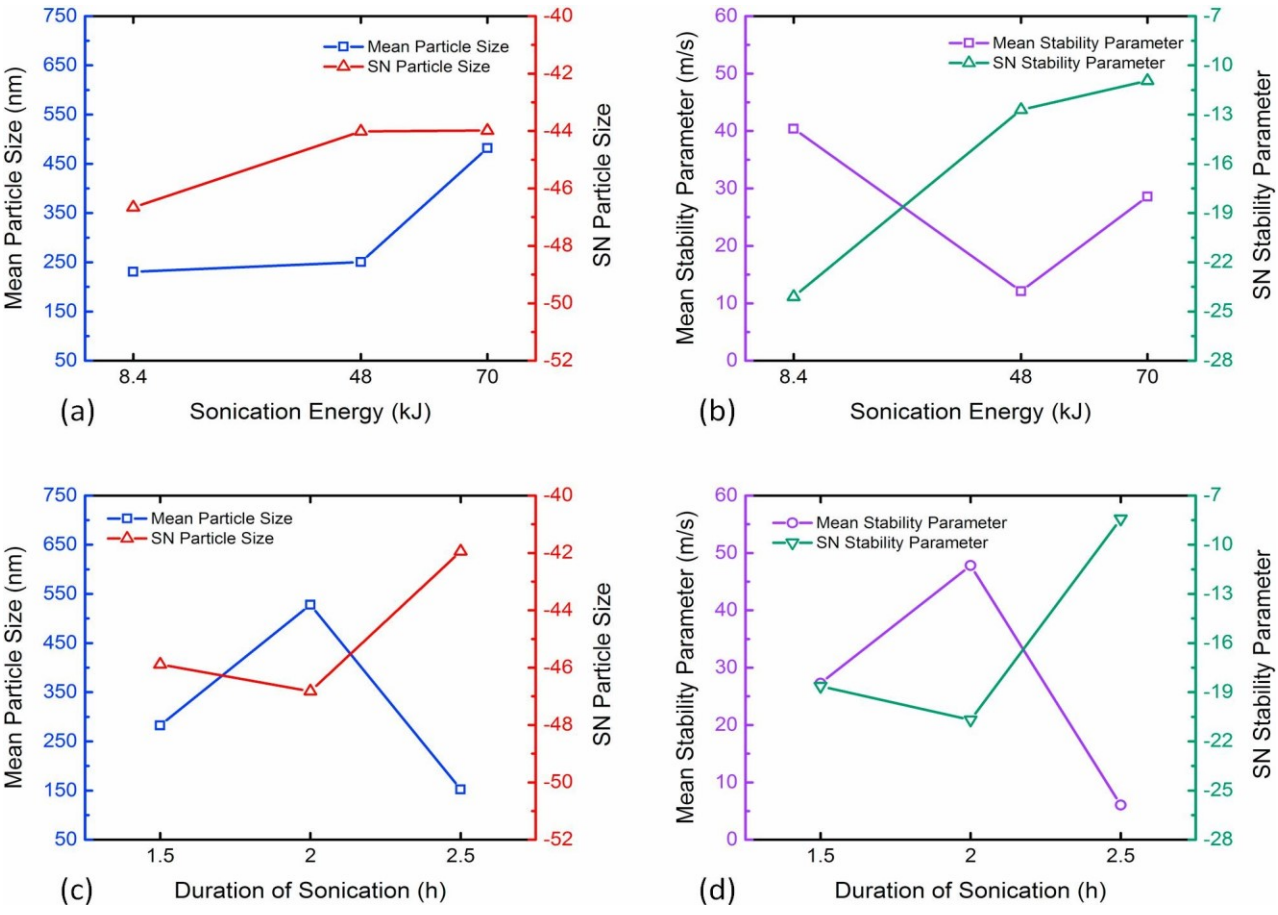

Figure 2.7: Effect of (a,b) sonication energy and (c,d) duration of sonication on mean responses and SN ratios for particle size and stability.

f) Effect of the temperature of the sonication bath

The preparation of a well-dispersed NPs suspension using a high-intensity probe sonicator requires careful adjustment of the temperature of the mixture. Controlling the temperature restricts the evaporation of the solution during sonication and thus prevents any change in the final composition of materials in the NPs suspension. Furthermore, the localized temperature caused by the cavitation during sonication may reach up to several thousands degree Kelvin which can affect the chemical composition and functional groups of the NPs [53]. There is some evidence that suggests the cavitation cycles related to the expanding and collapsing of micro-bubbles generate hot spots where NPs transiently experience extreme temperature and pressure condition (~5000 K and 1800 atm) [107–109]. This extreme condition can break up the aggregated NPs and provide a more uniform dispersion of NPs on the one hand. On the other hand, the very high localized temperature coupled with the high-intensity cavitation could initiate shock waves in the suspension that leads to the high-energy collision among NPs. This phenomenon may induce melting at the point of collision and thus increase the average particle size [107,110,111]. The effect of changing the temperature of the sonication bath on the size and stability of the resulting NPs are presented in Figures 2.8a and 2.8b. It can be observed that increasing the temperature of the sonication bath up to 18.5 °C increased the size of the NPs and their aggregation rate. Further increase of temperature decreased the size of the NPs. This result can be attributed to the counter-effects of generated shock waves at hot spots and melting of the collision points.

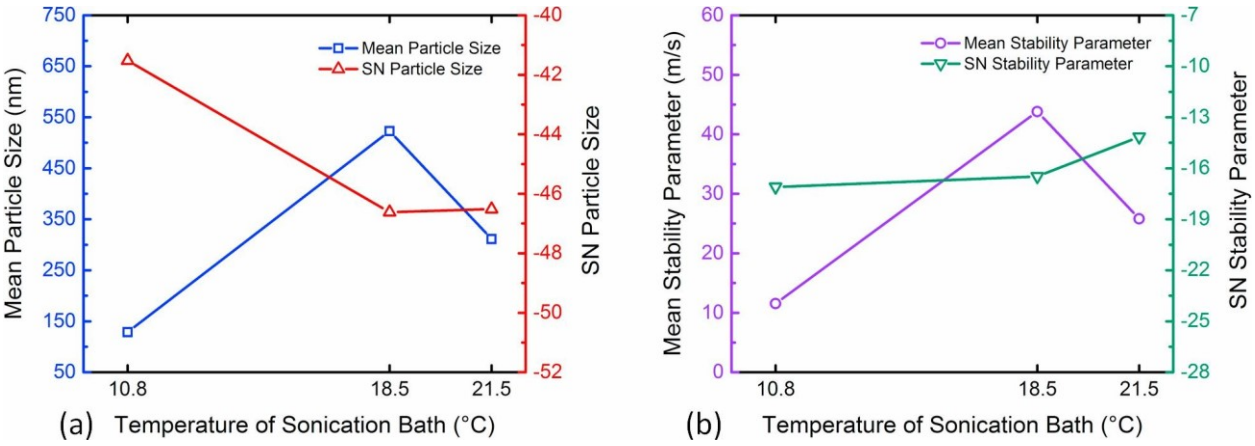

Figure 2.8: Effect of the temperature of the sonication bath on the (a) particle size and (b) stability and their corresponding SN ratios.

g) Effect of length of shaking of the NPs suspension

Figure 2.9 demonstrates the effect of the length of the shaking of the NP suspension on the size and stability of NPs. Based on ANOVA results in Tables 2.3 and 2.4, manual shaking of the NPs suspension at different time interval had a significant effect on the size of NPs while it did not influence the stability of the NPs suspension. As can be observed in Figure 2.9a, the increase in the length of shaking significantly decreased the size of NPs. A similar observation was also reported for the preparation of pharmaceutical NPs where the duration of shaking was found an effective parameter in reducing the size of NPs and improving the uniformity of sonicated suspensions [61]. A study comparing shaking and sonication for disrupting soil aggregates found that shaking was initially more effective for breaking down weaker aggregates, whereas sonication was found to be more efficient for stronger and more stable aggregates [112].

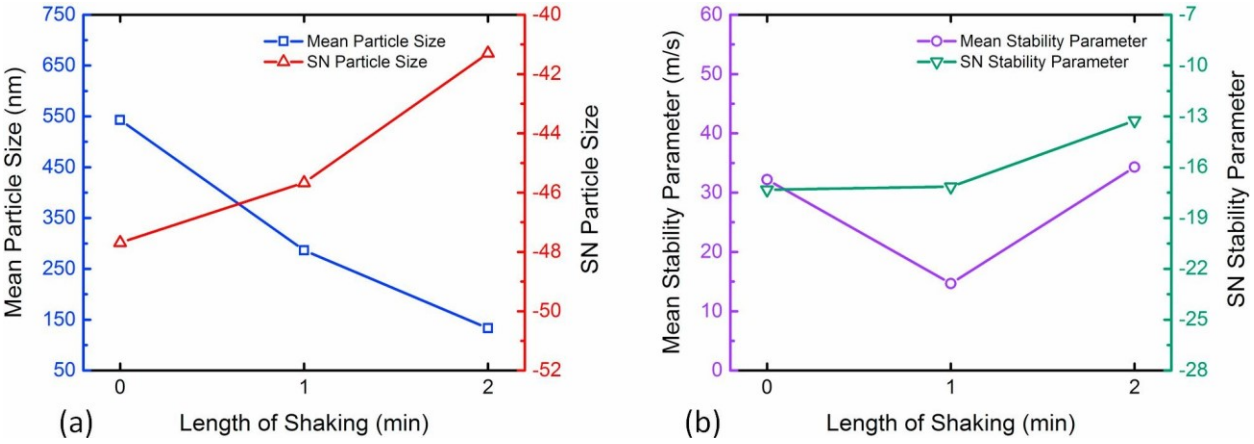

Figure 2.9: Effect of duration of shaking on mean responses and SN ratios for (a) particle size and (b) stability.

2.3.4 Optimal setting of the control factors and confirmation experiments

The optimum combination of factor levels to obtain the most stable NPs dispersion with the lowest particle size can be identified by employing either the mean response plot and the plot of SN ratios. Regarding the mean plot in Figures 2.3 to 2.9, the optimal level settings are the lowest data points in the mean response (particle size and stability parameter) plots and the highest ones in the SN ratio plots. The trend of change on these two plots satisfactory matches

each other except for insignificant control factors (the immersion depth of the probe and the intensity of sonication for the plot of mean particle size and the intensity of sonication, the temperature of sonication bath and the length of shaking for the plot of stability parameter). Figure 2.10 demonstrates the particle size and the size variation over time of a confirmation test which was prepared based on the optimal levels of the control factors suggested by the SN ratios. The optimum levels of the control factors are also presented in Figure 2.10 which are (i) 7.5 mm for the immersion depth of the sonication probe, (ii) 30 ml of heptane, (iii) 10.8 °C for the temperature of the sonication bath, (iv) 70 kJ for the sonication energy delivered to the suspension, (v) 150 min for the duration of sonication which included five 30-minute sonication increments, (vi) 2 minutes of shaking of the NPs suspension between each sonication increments, (vii) 0.6 g of solid ITO NPs, and finally (viii) 100 µl of BYK as dispersing agent. It can be observed that a stable and well-dispersed NPs suspension was obtained by optimizing the levels of the control factors. The surface (zeta) potential of ITO NPs at this optimum level was measured to be 0.20±1.51 mV which reveals the dominant role of steric stabilization compared to electrostatic repulsion.

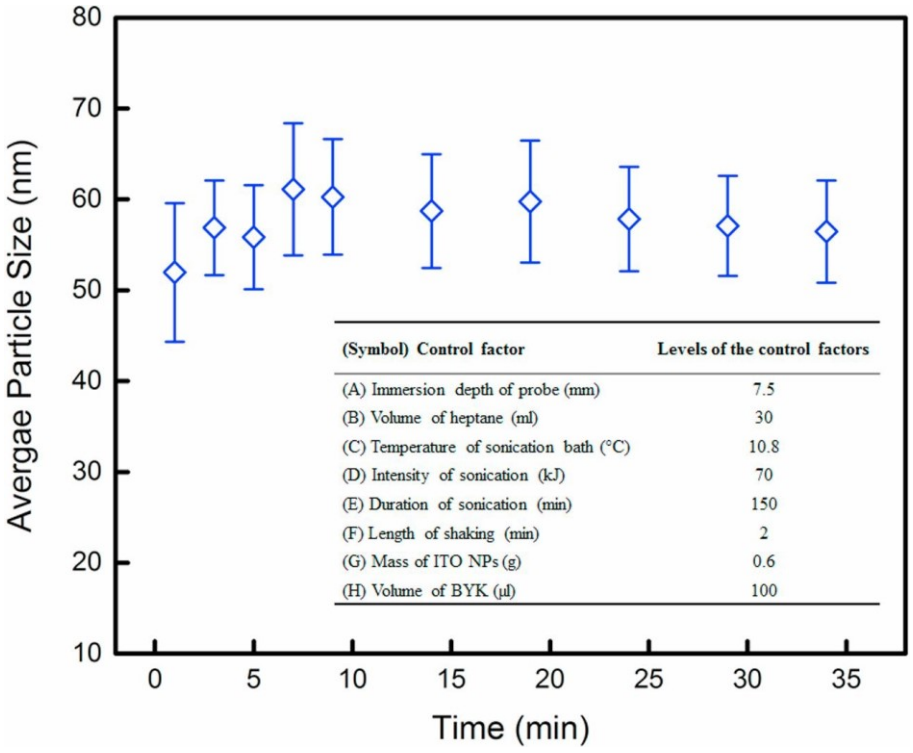

Figure 2.10: Optimized experimental results for particle size based on the plot of SN ratios.

Figure 2.11 shows the characterizations results of solid ITO NPs and the NPs suspension prepared based on the optimal setting of the control factors. Panel (a) in Figure 2.11 presents the FESEM images of the synthesized solid ITO NPs showing an agglomerated structure of the NPs with a size distribution below 100 nm. The elemental composition of the synthesized ITO NPs were obtained by EDX and the spectrum was presented in panel (b). Panel (c) demonstrates the TEM images of the optimized ITO NPs suspension. The TEM image shows the small size of ITO NPs and the absence of large aggregated clusters in the suspension. The presence of a single peak at 60 nm in the graph of size distribution in panel (d), confirms the preparation of well-dispersed suspension at the optimum levels of control factors. The size and stability of the confirmation sample were measured again three, five and seven days after the experiment, and the size remained within the range of 45-70 nm, which indicates the high stability of the optimized dispersion of the ITO NPs in heptane.

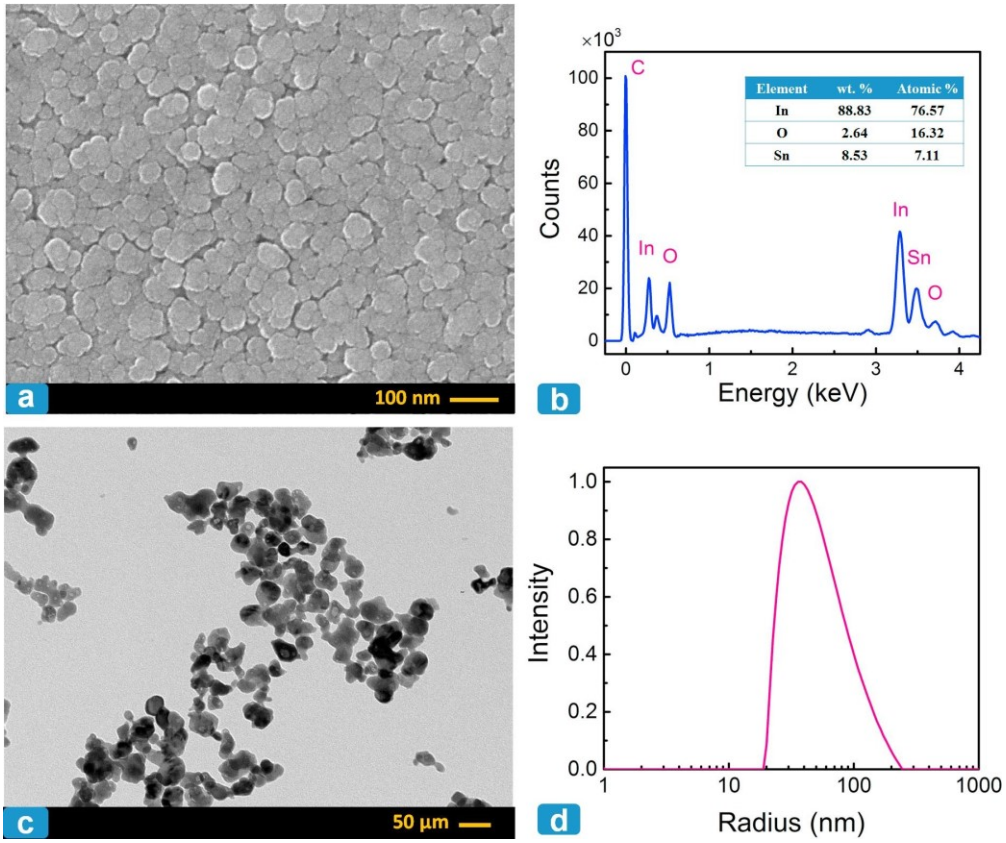

Figure 2.11: (a) FESEM image of the solid ITO NPs, (b) EDX elemental composition of the synthesized ITO NPs, (c) TEM image of ITO NPs dispersion for the optimal confirmation test, (d) initial particle size distribution of the ITO NPs obtained by DLS for the optimal confirmation test.

2.4. Conclusion

In the present study, well-dispersed and stable suspensions of nano-size ITO NPs were successfully prepared in heptane. In order to achieve this goal, the effects of eight dispersion parameters on the size and stability of ITO NPs were systematically investigated. Using an L_{18} Taguchi design, the synergistic effects and significance of control factors were studied, and the optimal levels were found. Significant factors for particle size, in the order of significance, were identified to be the volume of heptane, the volume of dispersing agent, the length of shaking the NPs suspension, the mass of ITO NPs, the temperature of the sonication bath, and the duration of sonication. Regarding the stability of the NPs suspension, the significant factors were found to be the mass of ITO NPs, the volume of dispersing agent, the immersion depth of the sonication probe, the intensity of sonication, and finally the duration of sonication. The optimized levels, which were suggested by Taguchi analysis, has resulted in suspensions of 43.0-68.3 nm ITO NPs, which were stable for several days. The Taguchi design provided valuable insight into the significance level and effect of different parameters for effective dispersion of ITO NPs in an organic solvent. Further studies can also be conducted to analyze the interactions between these factors. The results of the present study can be used as a guideline for effective dispersion of a wide range of metal oxide NPs in organic solvents.

Chapter 3. The incorporation of indium tin oxide to create thin film nanocomposite membranes

3.1 Introduction

There are expected to be 29 countries in the world by 2025 that experience water scarcity [6]. In the Middle East, this problem is being addressed through desalination; countries like Kuwait, Qatar, Saudi Arabia, and the UAE rely on desalination for the majority of their water needs [6]. Desalination is not limited to the Middle East, over 300 million people globally rely on this technology for freshwater production [8]. The most popular method to treat seawater and wastewater for drinking water use is through membrane separation technology, specifically a combination of nanofiltration and reverse osmosis (RO) [9].

The two most common types of RO membranes are cellulose acetate membranes, and thin film composite (TFC) polyamide (PA) membranes [19]. Comparatively, TFC PA membranes demonstrate greater water flux, superior rejection of salts and organics, higher compaction resistance, and a broader operating range for temperature and pH, over cellulose acetate membranes [19]. TFC membranes are comprised of (1) an ultra-thin skin layer on top, which are ~100-300 nm thick and composed mostly from PA, and (2) a microporous substrate which provides support [26,113]. There is, however, still demand for a more energy efficient and fouling resistant membrane that can be used for a variety of applications including desalinating seawater [21].

This challenge can be addressed through modification of the ultra-thin skin layer. The most common skin layer modification techniques are chemical grafting of functionalized materials to the surface and the incorporation of nanofillers. Nanofillers have several advantages over chemical grafting, including better scale-up potential and a stronger attachment of added particles to the membranes surface, compared to functional materials which can be easily washed away during operation. Nanoparticles (NPs), owing to their small size, can significantly affect the properties of their resulting nanocomposite and have been shown to enhance mechanical strength, heat resistance, permeability, and electrical conductivity for a variety of applications [15,46,48–50]. The potential use of NPs in membrane technology is to improve selectivity, flux,

as well as, other desirable qualities such as thermal resistance, mechanical stability, and antibacterial properties of the membrane during water treatment [26–29,37]. The first integration of NPs into the PA layer of a TFC membranes was a study by Jeong et al. in 2007 [32]. They added NaA zeolite NPs into the PA layer of a TFC membrane, resulting in a thin film nanocomposite (TFN) membrane that showed an improvement in water flux of nearly double the base TFC membrane, without a sacrifice in rejection. This research inspired others to follow Jeong's methodology and to incorporate different NPs into the PA layer for improving flux without sacrificing rejection [33,34]. Likewise, the incorporation of various NPs into the PA layer has also shown to improve the TFC membranes mechanical strength, and antibacterial properties [35–37]. TFN membranes have been tested at an industrial scale and have shown water flux twice that of conventional TFC membranes with a salt rejection higher than 99.7% [26].

Some of the most commonly used NPs for TFC membranes include graphene, carbon-based nanotubes, and metal oxides [28,114]. Metal oxides, predominately titania, alumina, magnetite, silica, and zirconia, have been shown to increase the hydrophilicity of the membrane and thus flux, while also improving thermal stability and mechanical strength. [28]. Indium Tin Oxide (ITO) is a widely used transparent and conductive material that is used in the fabrication of LED's, solar cells, and optoelectronic devices [76,77]. The benefit of incorporating Indium Tin Oxide (ITO) into TFC membranes yet to be explored, despite evidence by Khorshidi et al. that the incorporation of ITO into the polymer matrix of phase inversion membranes for water treatment enhanced the flux, conductivity, antifouling properties, and thermal stability [38]. This is due to the major challenge of dispersing the metal oxides in the non-polar organic solvent without causing severe aggregation of the NPs. However, in our previous work in chapter 2, we were able to properly disperse ITO NPs in the organic solvent that will be used in the synthesis of TFN/TFC membranes [115].

The objective of this work is to use stable and well dispersed ITO NPs to synthesize ITO TFN membranes, test them in both RO and Forward Osmosis (FO) setups, and compare them with the base TFC membrane. The membranes will be characterized using contact angle, zeta potential, and thermogravimetric analysis; as well as imaged at the surface and the cross-section by SEM and TEM.

3.2 Materials and Methods

3.2.1 Materials

ITO NPs were synthesized in the lab using the same method and materials as outlined in Chapter 2 [115]. Polyethersulfone (PES) membranes, with a thickness of 120 µm and a pore size of 0.2µm were purchased from Sterlitech Corporation (Kent, Washington, USA). Trimesoyl chloride (TMC) and m-Phenylenediamine (MPD), used as the organic solvent and water monomer, were purchased from Sigma Aldrich. Also, triethylamine (TEA) and sodium dodecyl sulfate (SLS) were used as additives to the water monomer and were also purchased from Sigma Aldrich.

3.2.2 Synthesis of TFC and TFN membranes

TFN and TFC membranes were both prepared via interfacial polymerization (IP) to coat a layer of PA onto the surface of the PES support. This process is illustrated in Figure 3.. The synthesis of the TFC membrane was done by first mounting the PES support onto a frame and then pouring a solution of MPD, along with TEA and SDS, in water and soaking the surface for 8 minutes. The excess MPD solution was then removed and a TMC solution was poured on top of the MPD soaked support to begin the polycondensation reaction. After a reaction time of 30s a thin PA layer of ~300 nm was formed. This membrane was then cured in an air-circulated oven at 60°C for 4 minutes.

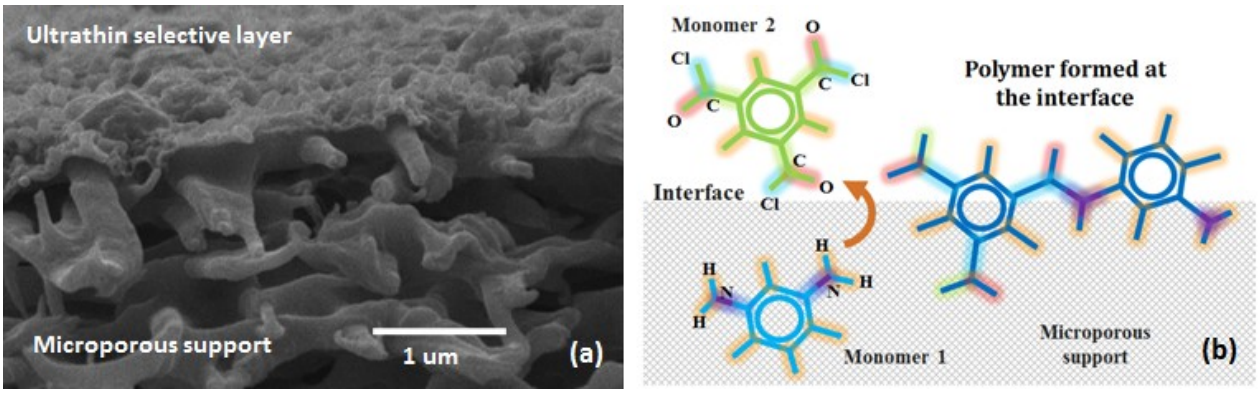

Figure 3.1: The formation of the PA layer atop a microporous support to form a TFC membrane. (a) is a cross-sectional FESEM image and (b) is the chemical reaction to form the PA layer where monomer 1 is MPD and monomer 2 is TMC.

The TFN membranes were prepared similarly with the difference being the presence of ITO NPs in the TMC solution. Before the addition of TMC during IP, a dose of three different volumes, 0.4, 1, and 2ml,of the ITO NP suspension was added to the TMC solution and sonicated for 4 minutes. The NP dispersion was a mixture of 0.6g ITO, 30 ml heptane, and 150 µl BYK-106, and was prepared via the optimal synthesis protocol in chapter 2 [115]. This TMC solution was then immediately added to create the IP reaction. There were two primary levels of ITO loadings in the membrane used in this paper 0.01% and 0.02%, created from a dose of 1 and 2ml of the ITO NP suspension, which will be referred to as TFN 1 and TFN 2 respectively. In addition, for RO testing an additional membrane prepared with 0.4% ITO was tested.

3.2.3 RO filtration flux measurement and rejection

The synthesized membranes were tested in a pressure-driven cross-flow membrane filtration setup (Sterlitech Co, CF042A cell, USA) similar to previous studies in our lab [18]; this is shown schematically in Figure 3.. In addition, the filtration setup consists of a stainless steel feed tank, a constant flow diaphragm pump with a maximum capacity of 6.8 LPM (Hyrda-Cell), temperature regulation done by a chiller/heater (Isotemp 3013, Fisher Scientific), a bypass valve and a back pressure regulator to control the pressure and cross-flow velocity (Swagelok), a digital weighing balance to measure the volume of the permeate (Mettler Toledo), and a data acquisition software named LabView to input the data directly into the computer (National Instruments).

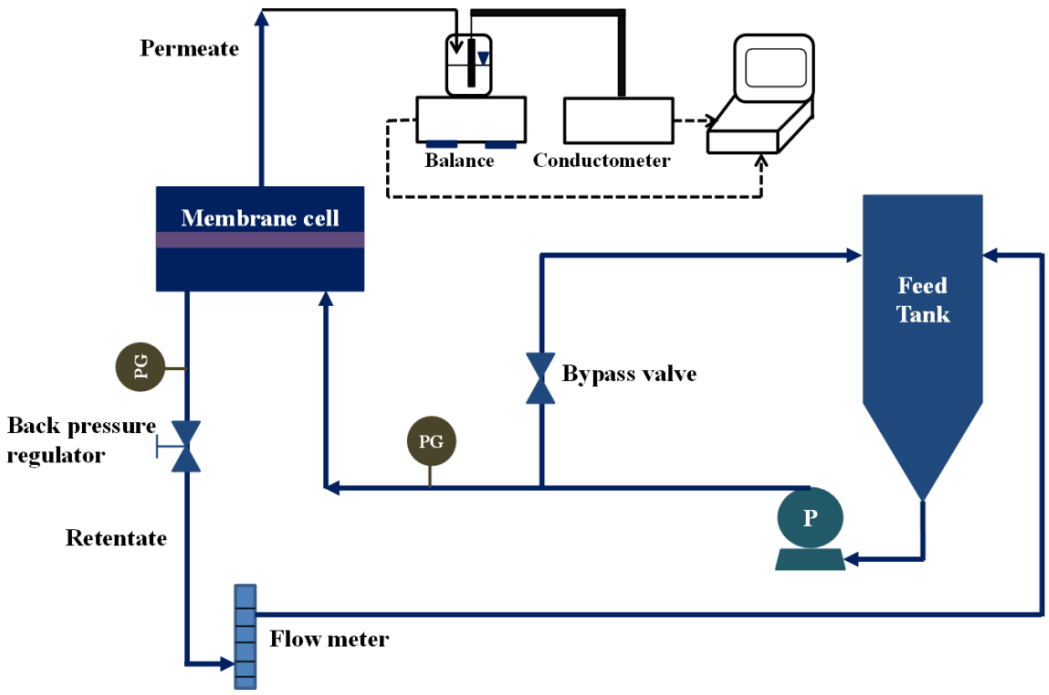

Figure 3.2: Schematic view of cross-flow RO pressure-driven filtration setup. Reprinted from [18] with the permission of Behnam Khorshidi.

The membranes were evaluated at steady state with an operating pressure of 220 psi, a feed flow rate of 1 $Lmin^{-1}$, and a water temperature of 25°C water. The water flux (J_w) was evaluated by measuring the change in the volume (V) of the permeate and dividing it by the time increment of measurement (t) and the filtration area of the membrane (A); this is shown in equation 3.1. The rejection (R) was evaluated by using the concentration of the salt in the permeate (C_p) and the concentration of salt in the feed (C_f) and is shown in equation 3.2.

$$J_W = \left(\frac{\Delta V}{At} \right) \tag{3.1}$$

$$R = (1 - \frac{C_p}{C_f}) \times 100 \tag{3.2}$$

The feed tank for measuring pure water flux was 5L of distilled water. For the measurement of saline water flux, after 30 minutes of recorded stead pure water flux, a mixture of 10g of NaCl in 50mL of distilled water was added to the feed and run for 3 hours.

3.2.4 FO filtration flux measurement and rejection

The filtration performance of the membranes was also evaluated using a cross flow FO setup, similar to a previous study by Khorshidi et al. [113], which is shown schematically in Figure 3.. There are channels on both sides of the permeate cell (Sterlitech Co, USA) with one connected to the feed tank, and the other connected to the draw tank. The membrane cell has a larger surface area than that of the RO permeate cell; thus, for FO testing, a slightly larger membrane was synthesized using the same amount of solution.

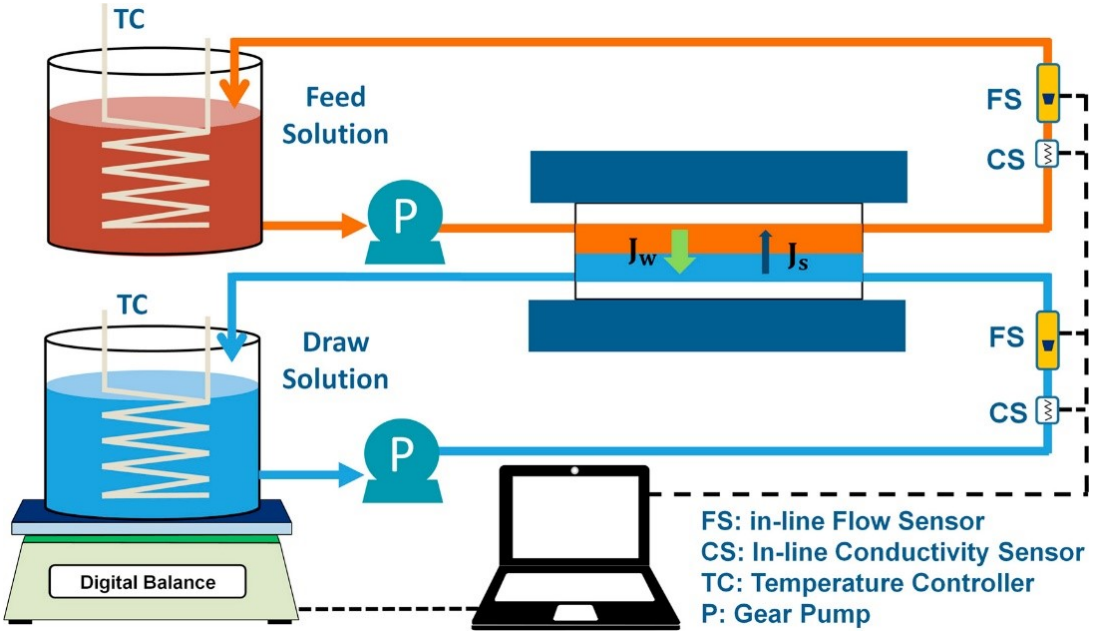

Figure 3.3: Schematic view of cross-flow FO concentration-driven filtration setup. Reprinted from [113] with the permission of Elsevier.

Water flux was measured through the use of salt water with an NaCl concentration of 0.5M for the draw solution, and distilled water for the feed solution. A volume of 2.9L was used for the draw side and 3L was used for the feed side. The system was run for 5 minutes with only distilled water to stabilize the flow, before the addition of an NaCl solution to the draw side. Samples were taken from the feed and draw side every 30 minutes, and their conductivity was measured. The experiment was run for a total of 2.5 hours. The change in mass (m) in the draw tank was measured using a digital balance and the FO flux, J_{W_FO}, was calculated using equation 3.3:

$$J_{W\_FO} = \left(\frac{\Delta m}{\rho A \Delta t} \right) \tag{3.3}$$

where ρ is the density of the draw solution, A is the membrane surface area, and t is the change in time. In addition to measuring the flux of water molecules from the feed tank to the draw tank, the reverse flux of salt, J_s, from the draw tank to the feed tank was calculated using equation 3.4:

$$J_s = \left(\frac{C_{f,t}(V_{F0} - J_{W\_FO} A t}{At} \right) \tag{3.4}$$

where $C_{f,t}$ is the NaCl concentration of the feed at time t, V_{F0} is the initial volume of the feed solution.

3.2.5 Other Characterization Techniques

a) Microscopy techniques

To obtain images of the membranes surface and cross-section, field emission scanning electron microscopy (FESEM) (Zeiss Sigma 300 VP) and transmission electron microscopy (TEM) (Philips/FEI Morgagni 268, The Netherlands) were used. TEM was used to obtain cross-sectional views of the membrane, showing the dispersion of NPs inside the PA layer as well as the thickness of the PA layer. The thickness of the PA layer was taken as the average of 6 measurements. FESEM was used to take images of the surface morphology of the membrane and show the dispersion of the nanoparticles across the surface.

b) Elemental analysis

Elemental analysis was conducted using an energy-dispersive X-ray spectroscopy acquisition system (EDX) (Bruker) to determine the chemical composition of materials at the surface of membranes.

c) Contact angle

The hydrophilicity of the membranes was further evaluated using contact angle (Krüss Drop Shape Analyzer, Germany). The membrane was placed flat on a surface, and the static

contact angle of a drop of ultra-pure water was placed on the membrane in at least four different locations, and an average contact angle measurement of the water droplet on the membrane surface was obtained.

d) Zeta potential

To test the effect of the addition of ITO into the membrane's PA layer, zeta potential measurements of the membranes were done using a Surpass 3 (Anton Parr). The zeta potential of the NPs themselves was also evaluated using a Malvern Zetasizer Nano ZSP (Worcestershire, UK). The NPs were dispersed in water before measurement.

e) Thermal stability analysis

Thermal gravimetric analysis (TGA) was done on the fabricated membranes to measure its thermal stability. TGA measures the change in weight of the sample in relation to a changing temperature. 10 mg of the membrane was placed in the sample holder of the TGA Q50 (TA Instrument, Newcastle, Delaware, USA), and the temperature was increased to 700°C, with a slope of 10°C/min, and the change in weight of the sample was recorded. Similar to other studies, the decomposition temperature (T_d) of the TFN membrane was defined as the temperature after a 3% weight loss [116].

3.3 Results and Discussion

3.3.1 Membrane morphology

Cross-sectional imaging of the membranes was done through TEM, and is shown in Figure 3. The addition of ITO NPs shows a significant increase in the thickness of the PA layer, as indicated by comparing the growth of the PA layer in images 1a-1c in Figure 3. This can be attributed to the decrease in the concentration of TMC due to dilution of the organic solvent in the synthesis process with the addition of the ITO-heptane solution. A reduction in the concentration of TMC, in the interfacial layer reaction with MPD, will more readily permit diffusion of the MPD molecules towards the organic solvent, increasing the thickness of the PA layer [117]. Another explanation for the increased thickness of the PA layer is the possible interactions caused by the BYK-106 molecules (utilized surfactant for the dispersion study) that

were present in the ITO-heptane solution. The presence of BYK at the interface of the two monomers might have decreased the interfacial tension between the heptane and the water [88]. This will allow for faster diffusion of MPD into the organic phase, and subsequently an increased thickness of the PA layer. Imaging also shows that when comparing these membranes, there appears to be a slight decrease in the density of the PA layer.

Figure 3, images 1c and 2c, show well integration of the ITO NPs into the PA layer ridge and valley structure of TFN 2. Figure 3, images 1b and 2b, however, show a location where the integration of ITOs NP in TFN 1 were predominately found on the surface as opposed to well embedded throughout the thickness of the PA layer. In all cases, imaging shows that the additional growth of the PA layer did not result in apparent voids along the cross-section of the membrane that would allow a significant increase in salt passage. This is evidenced by the lack of gaps in the ultra-thin PA layer above the microporous support.

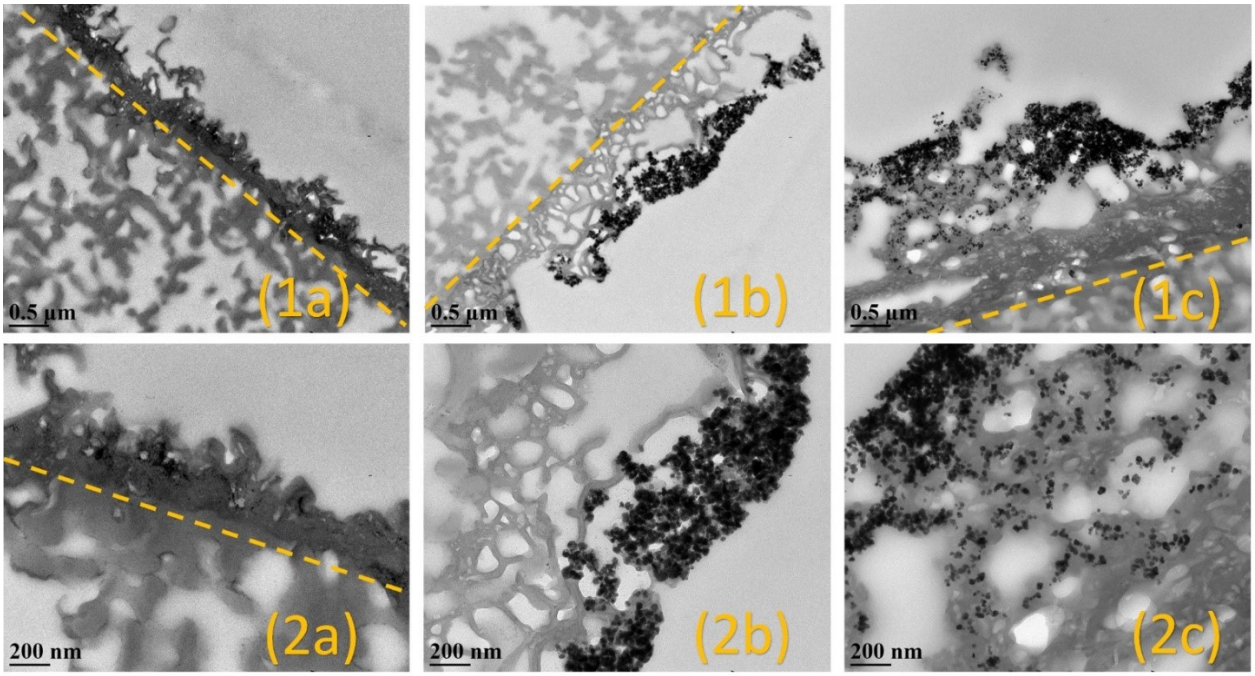

Figure 3.4: TEM cross-sectional images of the different membranes. (a) Is the base TFC membrane, (b) is the 0.01% ITO TFN 1 membrane, (c) is the 0.02% ITO TFN 2 membrane. (1) Is with a magnification of 22,000, (2) is with a magnification of 56,000. The dashed line indicates the separation between the PES sublayer and the PA layer, the entirety of (2b) and (2c) is a magnification of the PA layer.

The surface of the membranes was imaged using SEM. Image (a) of Figure 3.5 shows the SEM image of the base TFC membrane, and is a view of the PA layer without the addition of ITO. Image (b) of Figure 3.5 shows a larger cluster of NPs on the surface of TFN 1 in comparison to a more layered structure with TFN 2 in image (c) of Figure 3.5. The layered structure of TFN 2 can likely be attributed to more readily diffused MPD molecules through the organic solvent due to a decreased TMC concentration. Image c in Figure 3.5 confirms the well integration of the NPS in the ITO TFN 2 membrane through its layered structure.

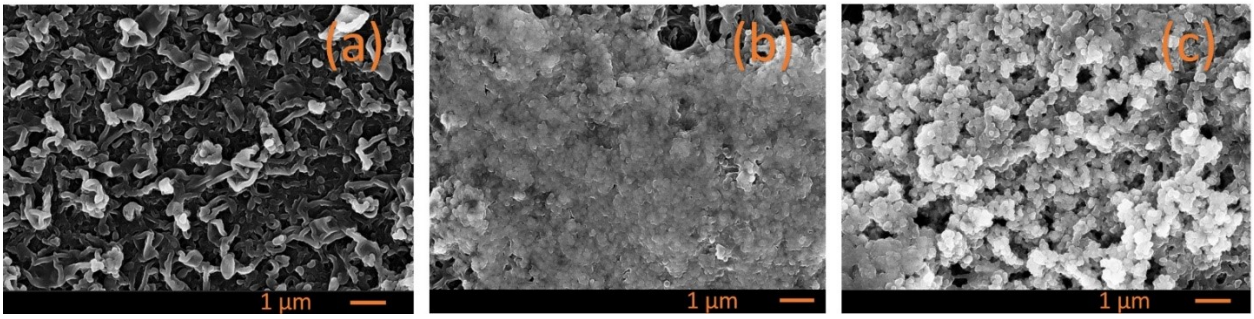

Figure 3.5: FESEM images of the (a) base TFC membrane (b) TFN 1 and (C) TFN 2 at a magnification of 10,000

The elemental composition of the membranes surfaces was found using EDX, and the results are shown in Figure 3.. Images (1a-c) show the elemental composition of a larger area of the membranes taken by the SEM at a magnification of 500x. The tables in these images show that the addition of NPs caused an increase in the wt.% of indium and tin from 0% in the base TFC membrane, to 25.9% and 0.5% in TFN 1, and 42.5% and 5.6% in TFN 2. Images (2a-c) show the elemental composition of a zoomed-in/magnified region as opposed to the entire FESEM picture, and images (3a-c) show the corresponding elemental composition plot. Despite an increase in the wt% of indium and tin between TFN 1 and TFN 2 in 500x magnification, at 5000x magnification the results were similar. This indicates that the addition of twice the amount of ITO solution did not result in more aggregation of the NPs at the surface.

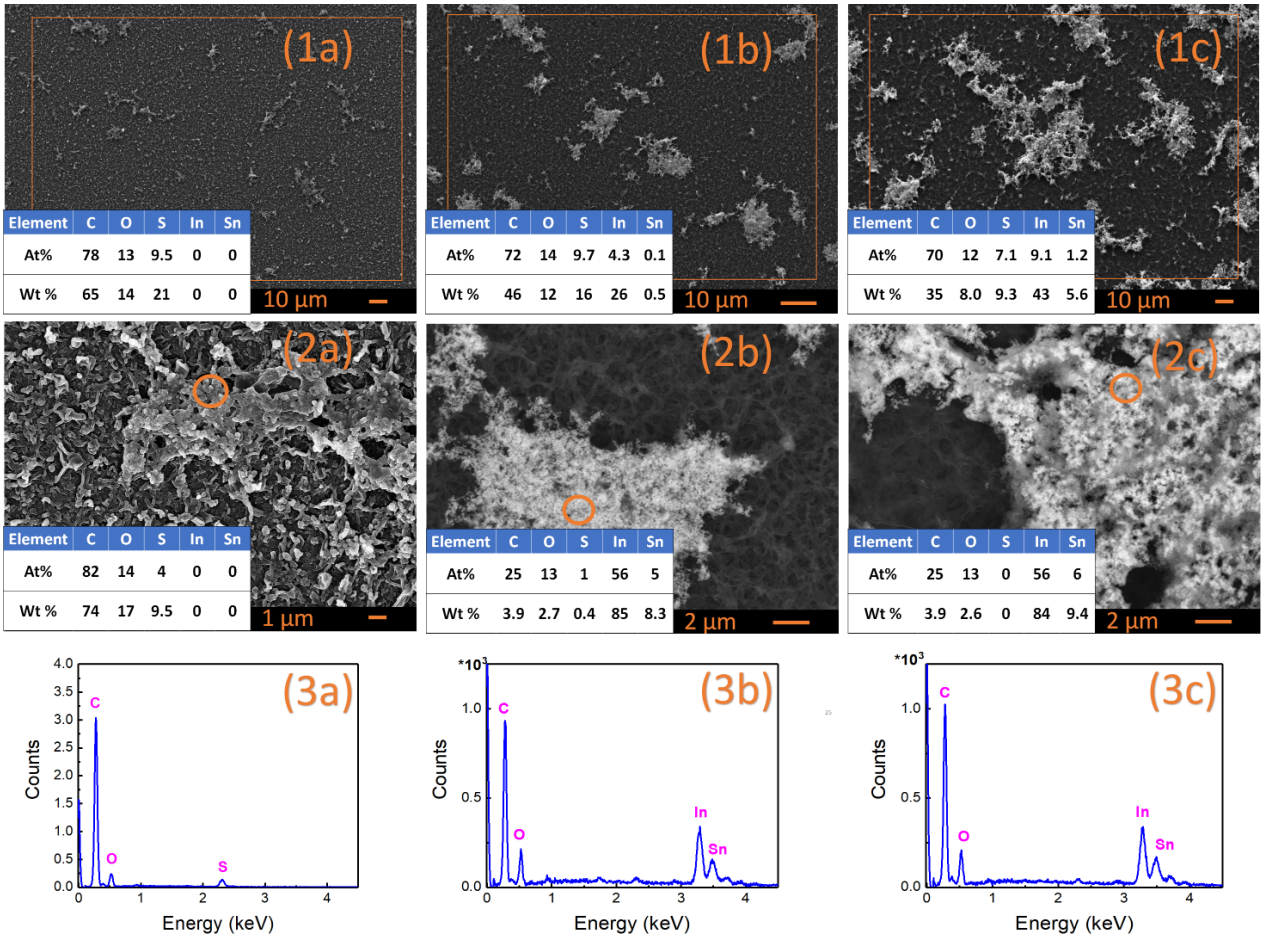

Figure 3.6: SEM+EDX images of the (a) base TFC, (b) TFN 1, and (C) TFN 2.The tables in images 1a-2c show the atomic (at) % and weight (wt) % of each element. Images (1a-c) are at a magnification of 500x and the EDX is of the entire image. Images (2a-c) are at a magnification of 5,000x and EDX is only of a specific region highlighted by the orange circle. Images (3a-c) are the accompanying elemental distribution plots.

3.3.2 Contact angle

Contact angle measurements of the ITO TFN membranes and the base PA/PES membrane are shown in Figure 3.. The addition of ITO is shown to increase the hydrophilicity of the membrane, as shown by a decreasing contact angle. The contact angle of the base membrane is 112.0°, 0.1% ITO TFN has a contact angle of 88.8°, and 0.2% has an angle of 70.8°. This can be attributed to the higher affinity of metal oxides to water [118]. The addition of these metal oxides at the surface improves the water molecules interaction strength to the membrane surface due to the formation of hydrogen bonds [118]. A greater adhesion force between the membrane

surface and the molecules, with a constant cohesion force between the water molecules, will result in a more hydrophilic surface [119].

These results indicate that the ITO TFN membranes can potentially provide better antifouling properties, as an increased hydrophilicity of the membrane decreases the severity of membrane fouling [15]. This can be explained by an increased vulnerability of hydrophobic membranes to hydrophobic interactions between the hydrophobic foulant and the membrane surface [120]

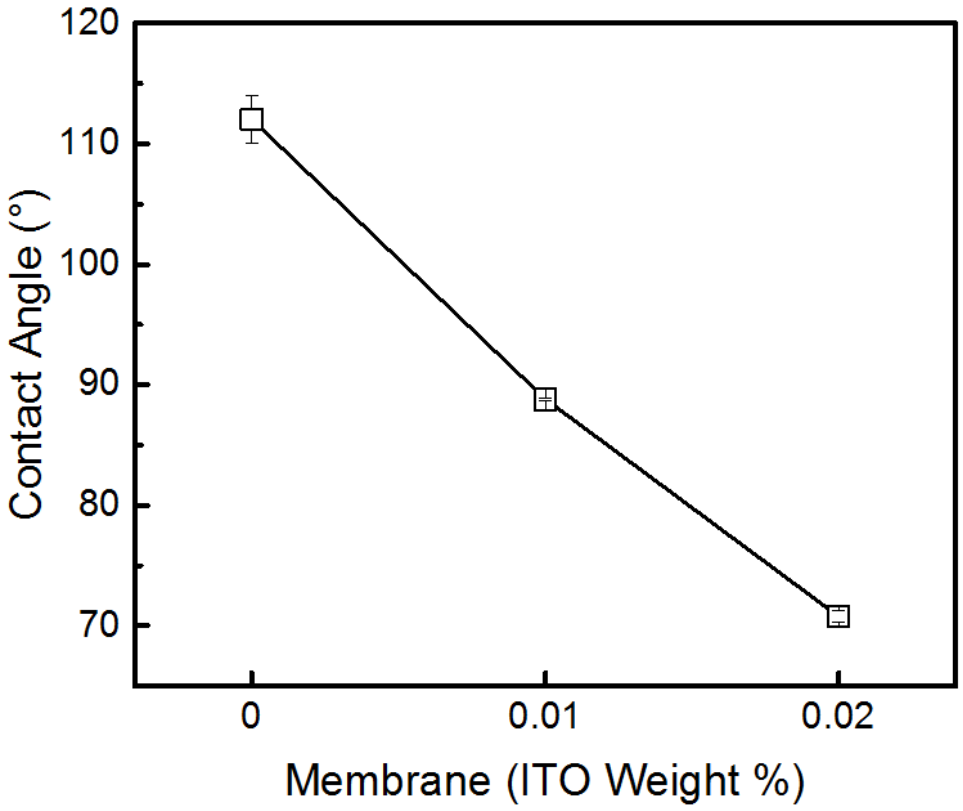

Figure 3.7: Increasing the weight% of ITO resulted in a decrease in contact angle at each level

3.3.3 Flux and rejection performance in RO and FO

The increased hydrophilicity of the TFN membranes, as shown by contact angle, indicate that the TFN membranes will demonstrate improved water flux during operation. The lack of any surface defects, as suggested by imaging of the membranes morphology, suggest that that increased water flux will not result in a diminished selectivity. This was confirmed in all tests, RO pure water in Figure 3., RO saline water in Figure 3, and FO flux in Figure 3. In addition to the hydrophilicity of the membrane, the flux and selectivity of the membrane is affected by different factors; including the size, shape, hydrophilicity, and dispersion quality of the NPs themselves, the thickness of the PA layer and morphology, and the ratio of NPs in the polymer matrix [27].

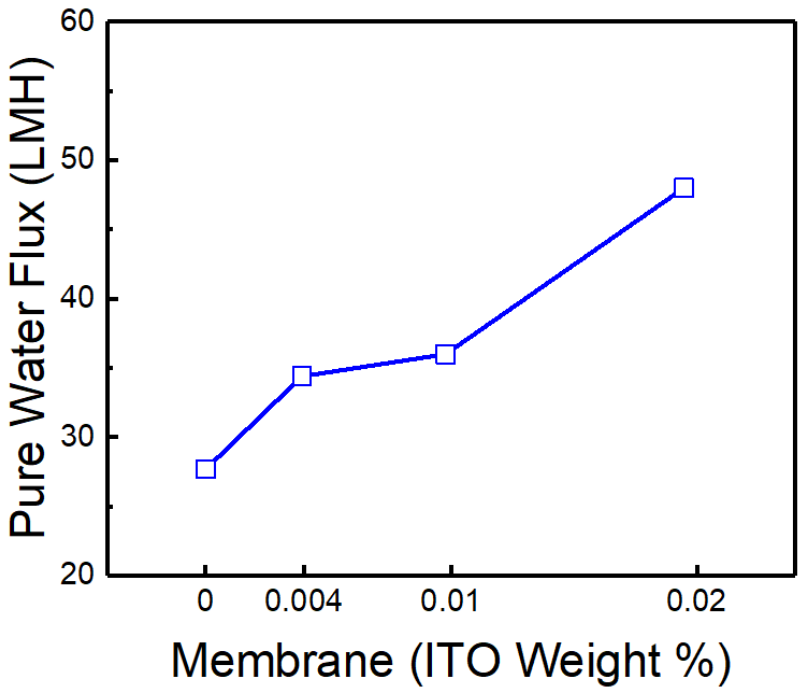

Figure 3.8: RO pure water flux results showing an improved flux with the addition of ITO

The increase in flux for RO pure water flux followed the expected trend, as demonstrated by a decrease in the contact angle for the addition of ITO. The effect of the improved hydrophilicity of the ITO TFN membranes is a cause of the increasing flux. The addition of salt to the feed was shown to drop water flux across each tested membrane, as expected. As shown in Figure 3, the water flux trend under saline conditions was identical to pure water results, and

TFN 2 showed a nearly double increase once again. The rejection of all membranes was very similar, around 98%. The constant rejection confirms what was conveyed through images of the membrane, i.e., the addition of the ITO did not result in any voids (defects) in the PA layer that would allow an increased passage of salt.

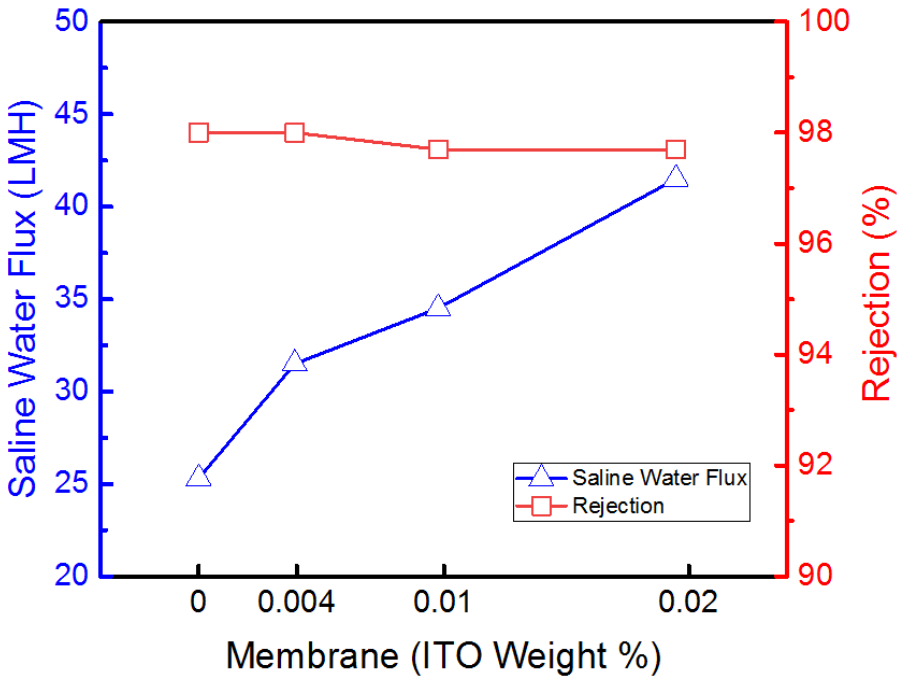

Figure 3.9: RO saline flux and rejection results showing the addition of ITO results in an improvement in flux without sacrificing selectivity

The permeation trend was repeated with the FO setup, as shown in Figure 3. The improvement of permeation flux from TFN 1 to TFN 2 was, however, minimal in the FO test. This could be a result of the larger surface area of the membrane inside the FO cell compared to the RO cell. This finding brings up the challenge of scaling up to commercial TFN membranes, as a larger surface area would increase the potential for the presence of defects. It also indicates that the optimal level of ITO loading lies between 0.01 and 0.02 wt%.

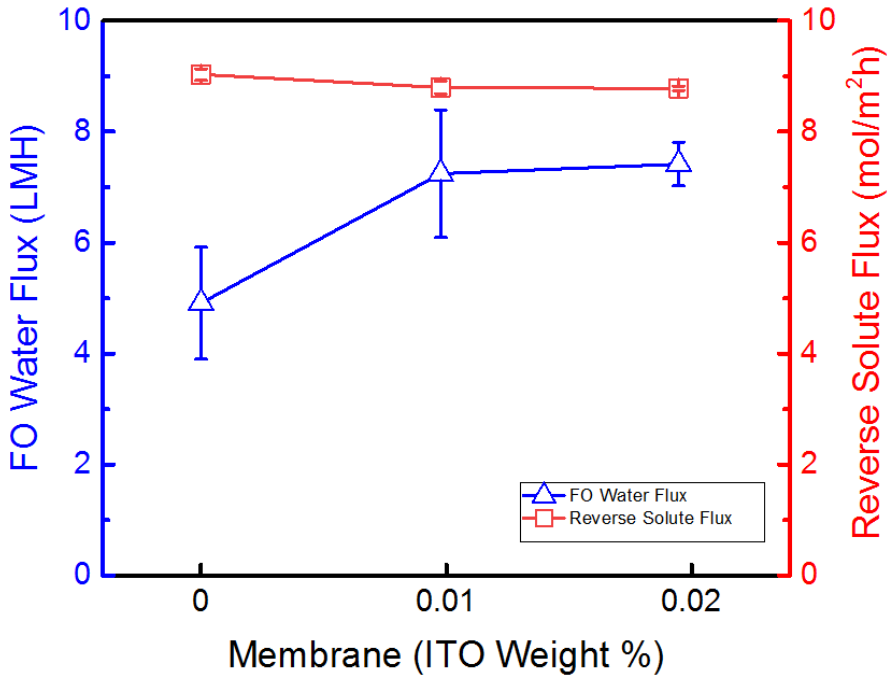

Figure 3.10: FO water and saline flux results showing another improvement for water flux with a small change in reverse solute flux

3.3.4 Zeta potential

The addition of ITO NPs was shown to increase the zeta potential of the membrane across all pH levels as shown in Figure 3. This could be attributed to the ITO NPs themselves, which have a more positive zeta potential compared to the PA layer. The zeta potential value for the ITO NPs dispersed in water was measured three times and the results were -9.60, -9.07, and -9.51 mV. The decreasing trend of the TFC's/TFN's zeta potential with an increasing Ph, in general, can be attributed to the amine functional groups [119]. A lower pH causes protonation of amine functional groups; this results in a more positive charge. At a higher pH, deprotonation of the amine functional groups along with dissociation of the carboxylic acid group or sulfonic acid group on the membrane surface.

Zeta potential measurements are determined on the basis of the Helmholtz-Smolchowski equation:

$$\zeta = \left(\frac{\Delta E \eta \kappa}{\Delta P \varepsilon \varepsilon_0} \right) \tag{3.5}$$

where ζ is the zeta potential, ΔP is the applied pressure, ΔE is the streaming potential, ε is the permittivity of the solution and free space, η is the solution viscosity and κ is the solution conductivity. One assumption made when using equation 3.5 that is not kept is that the surface conductivity has no effect and has homogeneous properties [119]. This assumption is not met because the surface of the TFN membranes contains conducive ITO NPs that are not distributed in a homogenous manner.

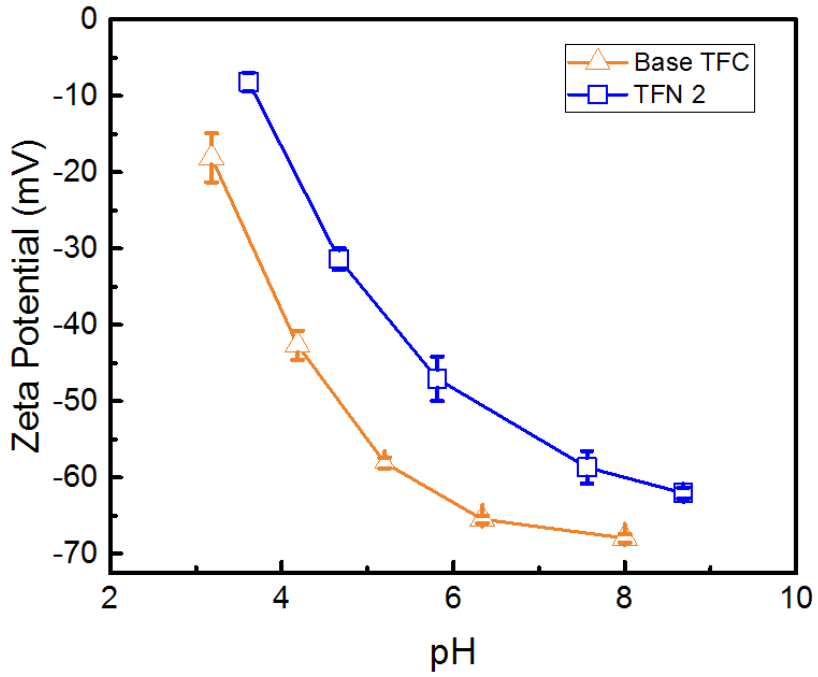

Figure 3.11: Zeta potential measurements showing a more positive shift in the pH zeta potential curve due to the presence of ITO

A more positive zeta potential may be beneficial during the removal of divalent positive ions such as calcium and magnesium. The removal of these divalent ions can play a role in reducing biofouling due to an increased potential for organic fouling due to their presence [121]. During seawater desalination, these divalent ions may react with both humic acid and alginate and increase their build upon the surface of the membrane [121]. For alginate, the divalent

calcium ions act as a connection between the alginate molecules that deposit onto the surface of the membrane [121]. Thus, a surface that is more likely to repel these positive divalent ions has potential benefit in seawater applications.

3.3.5 TGA analysis

Figure 3. shows the result of TGA analysis of the ITO TFN membrane. The results show that a loading of 0.02% was enough to increase the temperature degradation temperature. The decomposition temperature of the base TFC membrane was 455°C, whereas it was 472°C for the X% TFN membrane. The largest weight loss% difference occurs at 590° where the ITO TFN membrane was able to retain 12% more of its original weight than the base TFC membrane. This corresponds to literature that shows that the addition of NPs to PES membranes was able to increase thermal stability, and lower thermal degradation [116].

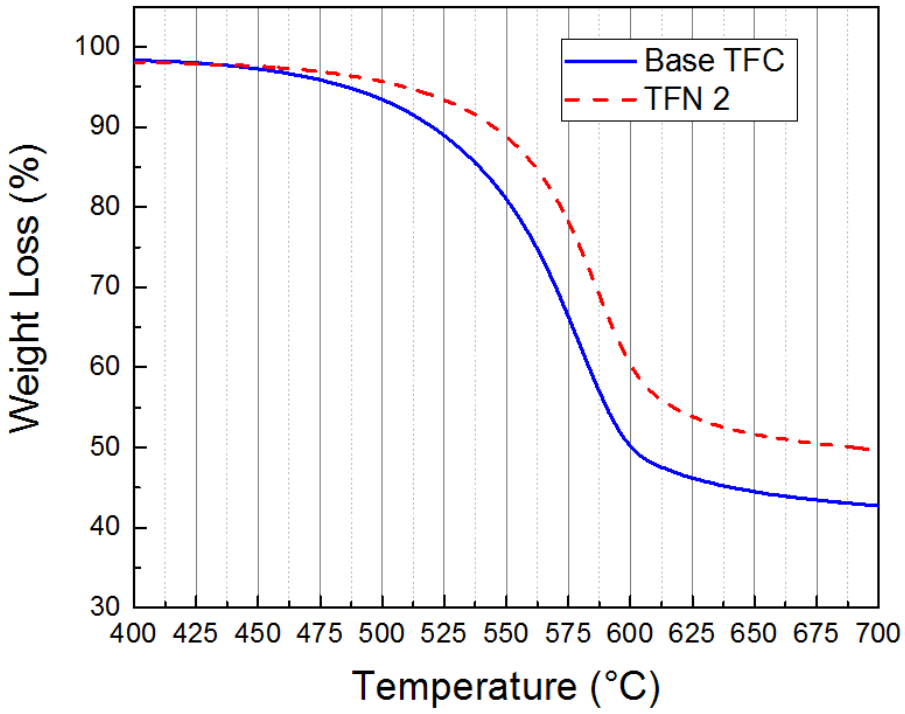

Figure 3.12: Weight loss of ITO TFN membrane as a function of temperature showing increased thermal stability of the ITO TFN membrane compared to the base TFC.

3.4 Conclusion

ITO was incorporated into TFC membranes and the resulting TFN membranes demonstrated superior water flux without a sacrifice in rejection in both pure and saline water for RO and FO. Although at each additional wt% of ITO there was an increase in flux for both RO and FO, there appeared to be a discrepancy in the optimal level. For future work, further experiments should be done to study this difference.

As a result of the ITO NPs, the TFN membranes also improved hydrophilicity, influenced a more positive zeta potential, and improved resistance to temperature degradation in comparison to the base TFN membrane. Surface and cross-sectional imaging of the membranes did not show any voids or defects created by the ITO NPs and was even able to show that the NPs were able to integrate well into the PA layer. The addition of an ITO solution during synthesis led to a decrease in the concentration of TMC, resulting in a thicker PA layer in the TFN membranes. Furthermore, the addition of ITO from 0.01 wt% to 0.02 wt% did not increase aggregation at the surface as demonstrated by EDX.

Chapter 4. Conclusion and future work

4.1 Conclusion

The research accomplished in this thesis was related the development of indium tin oxide (ITO)-based thin film nanocomposite (TFN) membranes, from fabrication and optimization of the dispersion of ITO nanoparticles (NPs) to their implementation onto the polyamide layer of thin film composite (TFC) membranes. The work was to originally start with the synthesis of defect free TFN membranes using ITO NPs to achieve an improved performance during flux measurements. However due to severe aggregation of ITO NPs in the organic solvent, a preliminary study was conducted to optimize the dispersion of nano-sized ITO NPs in heptane and this became the first part of the thesis. The second part of the thesis was the incorporation of well-dispersed NPs onto the surface of TFC nanofiltration (NF) and reverse osmosis (RO) membranes to improve their permeation properties and thermal stability.

Nanocomposites, formed from the incorporation of NPs into conventional materials, have been shown to exhibit improved properties, such as thermal, mechanical, and electrical properties over the conventional material. However, due to the nature of the small-sized NPs, a major challenge to proper utilization is their tendency to aggregate. The most commonly accepted method for dispersing NPs in a suspension is ultrasonication, however, there is no accepted standard procedure, and the optimal settings for each new dispersion must be found through experimentation [74]. The second chapter of this thesis found the optimal ultrasonication settings for synthesizing both a low size and stable NP dispersion of ITO in heptane. This was done by utilizing design of experiments (DOE), and more specifically a Taguchi L18 test, which evaluated the effect of each variable and recommended the optimal level to set the variable at. Eight factors were identified as influential and were studied: (i) the immersion depth of the sonication probe, (ii) the volume of the heptane, (iii) the temperature of the sonication bath, (iv) the intensity of sonication, (v) the duration of sonication, (vi) the length of shaking of the NPs suspension, (vii) the mass of ITO NPs, and (viii) the volume of the dispersing agent BYK-106.

The two overall most influential factors for both low size and stability were found to be the mass of ITO and the volume of BYK-106 in the dispersion. The significance of factors was found through analysis of variance (ANOVA). The significant factors for particle size according

to ANOVA were found to be, in order of significance, the volume of heptane, the volume of dispersing agent, the length of shaking the NPs suspension, the mass of ITO NPs, the temperature of the sonication bath, and the duration of sonication. For stability of the NPs suspension, the significant factors according to ANOVA were: the mass of ITO NPs, the volume of dispersing agent, the immersion depth of the sonication probe, the intensity of sonication, and finally the duration of sonication. The optimized levels, which were suggested by Taguchi analysis, were found to be: (i) a 7.5 mm for the immersion depth of the sonication probe, (ii) 30 ml of heptane, (iii) 10.8 °C for the temperature of the sonication bath, (iv) 70 kJ for the sonication energy delivered to the suspension, (v) 150 min for the duration of sonication which included five 30-minute sonication increments, (vi) 2 minutes of shaking of the NPs suspension between each sonication increments, (vii) 0.6 g of solid ITO NPs, and finally (viii) 100 µl of BYK as dispersing agent. This combination of factors results in ITO NP dispersions with a size of 43.0-68.3 nm that have been shown to be stable for over a week. Not only was this chapter successful in resulting in a stable enough suspension, and of a low enough size, to be used in the synthesis of TFN membranes, but the insights into the behavior of the factors during sonication can serve as a guideline for future work. When trying to disperse other NPs in the future, the path to a stable low size dispersion is more clear than before.

The addition of functional nanomaterials into the ultra-thin polyamide (PA) layer of TFC membranes with the aim of synthesizing high-performance nanocomposite membrane has recently garnered a great deal of attention. In addition to altering the flux and selectivity of the molecules that are able to pass through these membranes, these NPs have been shown to also be able to improve thermal stability and antibacterial properties. There has been a great deal of research on popular metal oxides such as titania, zirconia, and silica; but at the start of this thesis ITO was yet to be investigated. The third chapter of the thesis used the aforementioned stable dispersion of ITO in heptane to synthesize defect free ITO TFN membranes. These membranes were tested for both RO filtration, and FO filtration and the results showed an improvement in flux without a sacrifice in rejection due to an addition of ITO NPs in the PA layer at three weight percentages (0.004%, 0.01%, and 0.02%). The membranes were imaged using TEM, FESEM, and EDX. Additionally, contact angle, zeta potential, and thermogravimetric analysis were used for characterization.

TEM and FESEM images of the membranes both showed successful integration of the ITO NPs into the PA layer. Cross-sectional TEM images showed an increase in the thickness in the PA layer due to the addition of the addition of the ITO. There appeared to be no voids caused by the addition of ITO NPs in the ultra-thin PA layer according to TEM imaging, suggesting that the addition of ITO did not create any voids which would allow salt passage. FESEM images showed that increasing the wt% of the ITO NPs did not result in an increased aggregation of particles on the membranes surface. As evidenced by a decreasing contact angle, increasing the weight (wt)% of ITO NPs was able to increase the hydrophilicity of the membrane. This is attributed to the metal oxides ability to increase hydrogen bonding between water molecules and the surface of the membrane. As a result of this increase, the results for RO and FO both demonstrated that increasing the wt% of ITO resulted in an increase in water flux without decreasing the selectivity of the membranes. This confirms that the addition of ITO did not result in any defects in the PA layer.

In addition to flux and selectivity, the addition of ITO improved thermal stability, and also showed a positive increase in zeta potential. The increased zeta potential can result in a lower fouling rate of positive divalent ions, such as calcium and magnesium, during seawater filtration TGA results showed an improved resistance to thermal degradation with the addition of ITO, increasing the degradation temperature to 472° in the ITO TFN membrane compared to 455°

The objective set at the start of this thesis was met and ITO TFN membranes were successfully synthesized for the first time. This would not have been possible the work from chapter 2. The ITO TFN membranes were shown to have improved flux without a sacrifice in selectivity, improved thermal stability, and increased hydrophilicity compared to the base TFC membrane.

4.2 Future work

There are a several ways this thesis can be used as a base for future work; in addition to the knowledge gained in the optimization study. The first major way would be to continue with the methodology used in this paper and test ITO TFN membranes in more applications, specifically seawater and SAGD operation. The second way would be to use the knowledge gained in utilizing these conductive nanoparticles in electrofiltration.

The initial experiments outlined in chapter 3 are a strong indicator of the benefit of adding ITO to TFN membranes. However, using actual feed solutions of SAGD water and real seawater (SW) would be interesting and would further validate the results. This was not done due to time restrictions but would be perfect for showcasing the application of the work. With regards to SW, while pure salt water was tested in chapter 3, the composition of SW is different and includes more ions such as calcium, magnesium, chloride, and bicarbonate[122]. Table 4.1 shows an average of these ions found in SW as found by a study by Zhang et al., it is worth noting however that the composition of SW is not constant across the world and varies by region [122,123].

Table 4.1: Composition of SW

Ion Types	Na^+	K^+	Ca^{2+}	Mg^{2+}	Cl^-	HCO_3^-	SO_4^{2-}	Total Salinity
Concentration (mg/L)	1442.63	44.83	7.21	75.76	1195.71	2178.57	55.17	5000

The most common types of fouling during SW reverse osmosis (RO) are inorganic fouling (scaling), colloidal fouling, biological fouling, and organic fouling [16]. Inorganic fouling buildup on the membranes surface is due to the presence of divalent ions in the brine, colloidal fouling is caused by the suspended colloidal particles such as silica, biofouling is caused by living organisms, and organic fouling may result in hydrocarbon oil build up[16]. While the other three types of fouling are easy to identify, biofouling is a more complex issue with four stages [16,124]. The issue of biofouling caused by Algae is a major concern for Gulf countries such as the UAE and Oman, as these algae secrete extracellular polymeric substances composed of polysaccharides and proteins and can lead to the growth of bacteria [121,123]. The filtration of divalent ions may be improved by the changed zeta potential of the membranes by the addition of ITO, specifically the positive ions of calcium and magnesium, and is worth investigation. The presence of these divalent salts, specifically calcium and magnesium, can also interact with alginate from the algae as well as humic acid and increase fouling, therefore their removal will also help mitigate biofouling [121].

The treatment of SAGD water is one of great interest to industrial sponsors here in Alberta. As a result of industrial sponsorship, at our lab we have access to samples given straight from industry so there is no requirement to try and recreate the composition. The challenge, instead, would be with dilution and cleaning of the flux measurement systems after testing. Preliminary studies at our lab have shown that the inclusion of ITO into the polymeric matrix of the membrane have reduced fouling and improved performance of phase inversion membranes for treating SAGD water. A similar effect is expected for ITO TFN membranes and would show a great application of the work in this paper.

A popular method to mitigate fouling during membrane filtration is the application of an electric field during membrane filtration, this approach is known as electrofiltration [125–127]. An electric field is placed across the membrane by having a cathode and anode on opposite sides of the membrane and applying current. There are two electrokinetic phenomena which can improve the membranes filtration, electrophoresis and electroosmosis [126,127]. Electrophoresis is the movement of charged particles in a liquid, it is common for colloids in water to be negatively charged and the application of the electric field pushes these colloids away from the membranes surface and towards the cathode; thus reducing fouling [126,127]. Electroosmosis is the effect causing a liquid to move relative to a charged surface, or in this case the membrane surface; the cations along with the water move toward the cathode and cause an increase in the net flow of water from the anode to the cathode, thus increasing flux [126,127]. A study by Bayar et al. showed a 5-fold increase during filtration after the application of an electric field during the filtration of biological suspensions and tap water [127].

To improve the benefits of electrofiltration further, a new approach has emerged to use the membrane itself as the cathode [128,129]. The membrane was turned into a cathode by the addition of a stainless steel mesh inside of the flat sheet membrane with two anodes on either side of the membrane, approximately 1-2 cm away from the membrane with the application of current [128,129]. This type of system requires less energy to obtain the same electric field strength [126]. In addition to the potential benefits of electrofiltration, the incorporation of a mesh made of polyester itself was shown to have improved performance during FO filtration [130,131]. A novel approach could be taken to incorporate the stainless-steel mesh into the ITO membranes and, due to the conductivity of the ITO NPs, further increasing the potential for improved flux and reduced fouling.

4.3 Contributions

The work in this thesis has been successfully published and presented. The results of chapter 2 have been published in the Journal of Ultrasonics Sonochemistry [115]. A full citation and DOI and shown below.

Z. Almansoori, B. Khorshidi, B. Sadri, and M. Sadrzadeh, "Parametric study on the stabilization of metal oxide nanoparticles in organic solvents: A case study with indium tin oxide (ITO) and heptane," *Ultrason. Sonochem.*, vol. 40, no. September 2017, pp. 1003–1013, 2017.

https://doi.org/10.1016/j.ultsonch.2017.09.012

The results of chapter 2 along with some from chapter 3 have been orally presented at the 3rd International Conference on Desalination Using Membrane Technology in Gran Canaria, Spain under the title "Parametric study on the stability of indium tin oxide nanoparticles in organic solvent as a prerequisite for synthesizing defect-free thin film nanocomposite membranes". A link to the program manual is shown below:

https://www.elsevier.com/__data/assets/pdf_file/0005/274757/MDES2017_Oral-Programme_8-March.pdf

Finally, the results of this work were presented at the 2017 Ualberta 3-minute thesis competition and I received second place. The video can be found with the following URL: https://youtu.be/T1nwoMla8Ew

References

[1] UN, The human right to water and sanitation, (n.d.). http://www.un.org/waterforlifedecade/human_right_to_water.shtml (accessed August 30, 2017).

[2] UN, Sustainable Development Goals, (n.d.). https://sustainabledevelopment.un.org/?menu=1300 (accessed September 7, 2017).

[3] UN, Water, (n.d.). http://www.un.org/en/sections/issues-depth/water/ (accessed September 7, 2017).

[4] World Wildlife Foundation Canada, Freshwater, (n.d.). http://www.wwf.ca/conservation/freshwater (accessed September 7, 2017).

[5] E.W. Allen, Process water treatment in Canada's oil sands industry: I. Target pollutants and treatment objectives, J. Environ. Eng. Sci. 7 (2008) 123–138. doi:10.1139/S07-038.

[6] I. Bremere, M. Kennedy, A. Stikker, J. Schippers, How water scarcity will effect the growth in the desalination market in the coming 25 years, Desalination. 138 (2001) 7–15. doi:10.1016/S0011-9164(01)00239-9.

[7] Masdar, Water & The UAE, (n.d.). http://www.masdar.ae/en/intiatives/detail/water-the-uae (accessed March 27, 2016).

[8] Brian Bienkowski, Desalination is an expensive energy hog, but improvements are on the way, (2015). https://www.pri.org/stories/2015-05-15/desalination-expensive-energy-hog-improvements-are-way (accessed September 7, 2017).

[9] M.M. Motsa, B.B. Mamba, A. D'Haese, E.M. V Hoek, A.R.D. Verliefde, Organic fouling in forward osmosis membranes: The role of feed solution chemistry and membrane structural properties, J. Memb. Sci. 460 (2014) 99–109. doi:10.1016/j.memsci.2014.02.035.

[10] M. Mulder., Basic Principles of Membrane Technology, Kluwer Academic, 1997.

[11] T. Younos, K.E. Tulou, Overview of Desalination Techniques, J. Contemp. Water Res. Educ. (2005) 3–10. doi:10.1111/j.1936-704X.2005.mp132001002.x.

[12] W.E. Federation, Membrane Systems for Wastewater Treatment, McGraw-Hill, Alexandria, 2006.

[13] U. Zhanat, E. Sharipzhan, Mechanism of Gases Transfer through Polymer Membranes and

Membrane Module Calculation Model to Separate Gases, Procedia Technol. 1 (2012) 356–361. doi:10.1016/j.protcy.2012.02.074.

[14] M. Qasim, N.A. Darwish, S. Sarp, N. Hilal, Water desalination by forward (direct) osmosis phenomenon: A comprehensive review, Desalination. 374 (2015) 47–69. doi:10.1016/j.desal.2015.07.016.

[15] L.Y. Ng, A.W. Mohammad, C.P. Leo, N. Hilal, Polymeric membranes incorporated with metal/metal oxide nanoparticles: A comprehensive review, Desalination. 308 (2013) 15–33. doi:10.1016/j.desal.2010.11.033.

[16] S.S. Mitra, A.R. Thomas, G.T. Gang, Evaluation and characterization of seawater RO membrane fouling, Desalination. 247 (2009) 94–107. doi:10.1016/j.desal.2008.12.016.

[17] N. Maximous, G. Nakhla, W. Wan, Comparative assessment of hydrophobic and hydrophilic membrane fouling in wastewater applications, J. Memb. Sci. 339 (2009) 93–99. doi:10.1016/j.memsci.2009.04.034.

[18] B. Khorshidi, T. Thundat, B.A. Fleck, M. Sadrzadeh, A Novel Approach Toward Fabrication of High Performance Thin Film Composite Polyamide Membranes, Sci. Rep. 6 (2016) 22069. doi:10.1038/srep22069.

[19] D. Li, H. Wang, Recent developments in reverse osmosis desalination membranes, J. Mater. Chem. 20 (2010) 4551. doi:10.1039/b924553g.

[20] B. Khorshidi, T. Thundat, B. Fleck, M. Sadrzadeh, Thin film composite polyamide membranes: Parametric study on the influence of synthesis conditions, RSC Adv. 5 (2015) 54985–54997. doi:10.1039/C5RA08317F.

[21] M. Liu, S. Yu, J. Tao, C. Gao, Preparation, structure characteristics and separation properties of thin-film composite polyamide-urethane seawater reverse osmosis membrane, J. Memb. Sci. 325 (2008) 947–956. doi:10.1016/j.memsci.2008.09.033.

[22] D. Rana, T. Matsuura, Surface modifications for antifouling membranes, Chem. Rev. 110 (2010) 2448–71. doi:10.1021/cr800208y.

[23] W.J. Lau, A.F. Ismail, N. Misdan, M.A. Kassim, A recent progress in thin film composite membrane: A review, Desalination. 287 (2012) 190–199. doi:10.1016/j.desal.2011.04.004.

[24] D. Rana, T. Matsuura, R. Narbaitz, Novel hydrophilic surface modifying macromolecules for polymeric membranes: Polyurethane ends capped by hydroxy group, J. Memb. Sci. 282 (2006) 205–216. doi:10.1016/j.memsci.2006.05.024.

[25] B.J.A. Tarboush, D. Rana, T. Matsuura, H.A. Arafat, R.M. Narbaitz, Preparation of thin-film-composite polyamide membranes for desalination using novel hydrophilic surface modifying macromolecules, J. Memb. Sci. 325 (2008) 166–175. doi:10.1016/j.memsci.2008.07.037.

[26] W.J. Lau, S. Gray, T. Matsuura, D. Emadzadeh, J. Paul Chen, A.F. Ismail, A review on polyamide thin film nanocomposite (TFN) membranes: History, applications, challenges and approaches, Water Res. 80 (2015) 306–324. doi:10.1016/j.watres.2015.04.037.

[27] Tawfik Abdo Saleh and Vinod Kumar Gupta, Application of Nanomaterial-Polymer Membranes for Water and Wastewater Purification, in: Nanomater. Polym. Membr., 2016: pp. 233–250. doi:10.1016/B978-0-12-804703-3/00009-7.

[28] S. Hernandez, A. Saad, L. Ormsbee, D. Bhattacharyya, Ch 16. Nanocomposite and Responsive Membranes for Water Treatment, in: Emerg. Membr. Technol. Sustain. Water Treat., Elsevier Science, 2016: pp. 389–431. doi:10.1016/B978-0-444-63312-5.00016-4.

[29] S. Al Aani, C.J. Wright, M.A. Atieh, N. Hilal, Engineering nanocomposite membranes: Addressing current challenges and future opportunities, Desalination. 401 (2016) 1–15. doi:10.1016/j.desal.2016.08.001.

[30] J.W. Krumpfer, T. Schuster, M. Klapper, K. Müllen, Make it nano-Keep it nano, Nano Today. 8 (2013) 417–438. doi:10.1016/j.nantod.2013.07.006.

[31] L.B. Kim E. Sapsford, W. Russ Algar, Functionalizing nanoparticles with biological molecules: Developing chemistries that facilitate nanotechnology, Chem. Rev. 113 (2013) 1904−2074. doi:10.1021/cr300143v.

[32] B.H. Jeong, E.M. V Hoek, Y. Yan, A. Subramani, X. Huang, G. Hurwitz, A.K. Ghosh, A. Jawor, Interfacial polymerization of thin film nanocomposites: A new concept for reverse osmosis membranes, J. Memb. Sci. 294 (2007) 1–7. doi:10.1016/j.memsci.2007.02.025.

[33] J. Yin, E.S. Kim, J. Yang, B. Deng, Fabrication of a novel thin-film nanocomposite (TFN) membrane containing MCM-41 silica nanoparticles (NPs) for water purification, J. Memb. Sci. 423–424 (2012) 238–246. doi:10.1016/j.memsci.2012.08.020.

[34] B. Rajaeian, A. Rahimpour, M.O. Tade, S. Liu, Fabrication and characterization of polyamide thin film nanocomposite (TFN) nanofiltration membrane impregnated with TiO2 nanoparticles, Desalination. 313 (2013) 176–188. doi:10.1016/j.desal.2012.12.012.

[35] A. Nguyen, L. Zou, C. Priest, Evaluating the antifouling effects of silver nanoparticles

regenerated by TiO2 on forward osmosis membrane, J. Memb. Sci. 454 (2014) 264–271. doi:10.1016/j.memsci.2013.12.024.

[36] B. Yu, K.M. Leung, Q. Guo, W.M. Lau, J. Yang, Synthesis of Ag–TiO_2 composite nano thin film for antimicrobial application, Nanotechnology. 22 (2011) 115603. doi:10.1088/0957-4484/22/11/115603.

[37] M.M. Pendergast, E.M.V. Hoek, A review of water treatment membrane nanotechnologies, Energy Environ. Sci. 4 (2011) 1946. doi:10.1039/c0ee00541j.

[38] B. Khorshidi, J. Hajinasiri, G. Ma, S. Bhattacharjee, M. Sadrzadeh, Thermally resistant and electrically conductive PES/ITO nanocomposite membrane, J. Memb. Sci. 500 (2016) 151–160. doi:10.1016/j.memsci.2015.11.015.

[39] S. V. Sokolov, K. Tschulik, C. Batchelor-McAuley, K. Jurkschat, R.G. Compton, Reversible or not? Distinguishing agglomeration and aggregation at the nanoscale, Anal. Chem. 87 (2015) 10033–10039. doi:10.1021/acs.analchem.5b02639.

[40] Y. Rao, Nanofluids: Stability, phase diagram, rheology and applications, Particuology. 8 (2010) 549–555. doi:10.1016/j.partic.2010.08.004.

[41] M. Elimelech, Particle deposition and aggregation: measurement, modelling, and simulation, Butterworth-Heinemann, 1995. doi:10.1016/B978-0-7506-7024-1.50001-7.

[42] Y. Hwang, J.-K. Lee, J.-K. Lee, Y.-M. Jeong, S. Cheong, Y.-C. Ahn, S.H. Kim, Production and dispersion stability of nanoparticles in nanofluids, Powder Technol. 186 (2008) 145–153. doi:10.1016/j.powtec.2007.11.020.

[43] A. Ghadimi, R. Saidur, H.S.C. Metselaar, A review of nanofluid stability properties and characterization in stationary conditions, Int. J. Heat Mass Transf. 54 (2011) 4051–4068. doi:10.1016/j.ijheatmasstransfer.2011.04.014.

[44] E.M. Hotze, T. Phenrat, G. V. Lowry, Nanoparticle Aggregation: Challenges to Understanding Transport and Reactivity in the Environment, J. Environ. Qual. 39 (2010) 1909. doi:10.2134/jeq2009.0462.

[45] C. Ke, ed., Recent Advances in Nanotechnology, Apple Academic Press, 2011.

[46] K.J. Klabunde, R.M. Richards, Nanoscale Materials in Chemistry, 2nd ed., John Wiley & Sons, Inc., 2009.

[47] X. Luo, A. Morrin, A.J. Killard, M.R. Smyth, Application of nanoparticles in electrochemical sensors and biosensors, Electroanalysis. 18 (2006) 319–326.

doi:10.1002/elan.200503415.

[48] W.R. Caseri, Nanocomposites of polymers and inorganic particles: Preparation, structure and properties, Mater. Sci. Technol. 22 (2006) 807–817. doi:10.1179/174328406X101256.

[49] J. Kim, B. Van der Bruggen, The use of nanoparticles in polymeric and ceramic membrane structures: review of manufacturing procedures and performance improvement for water treatment., Environ. Pollut. 158 (2010) 2335–2349. doi:10.1016/j.envpol.2010.03.024.

[50] H. Lu, J. Wang, M. Stoller, T. Wang, Y. Bao, H. Hao, An overview of nanomaterials for water and wastewater treatment, Adv. Mater. Sci. Eng. 2016 (2016) 1–10. doi:10.1155/2016/4964828.

[51] K. Simeonidis, S. Mourdikoudis, E. Kaprara, M. Mitrakas, L. Polavarapu, Inorganic engineered nanoparticles in drinking water treatment: a critical review, Environ. Sci. Water Res. Technol. (2015). doi:10.1039/C5EW00152H.

[52] H. Althues, J. Henle, S. Kaskel, Functional inorganic nanofillers for transparent polymers., Chem. Soc. Rev. 36 (2007) 1454–65. doi:10.1039/b608177k.

[53] J.S. Taurozzi, V.A. Hackley, M.R. Wiesner, Ultrasonic dispersion of nanoparticles for environmental, health and safety assessment--issues and recommendations., Nanotoxicology. 5 (2011) 711–29. doi:10.3109/17435390.2010.528846.

[54] V.S. Nguyen, D. Rouxel, R. Hadji, B. Vincent, Y. Fort, Effect of ultrasonication and dispersion stability on the cluster size of alumina nanoscale particles in aqueous solutions, Ultrason. Sonochem. 18 (2011) 382–388. doi:10.1016/j.ultsonch.2010.07.003.

[55] I.M. Mahbubul, R. Saidur, M.A. Amalina, E.B. Elcioglu, T. Okutucu-Ozyurt, Effective ultrasonication process for better colloidal dispersion of nanofluid, Ultrason. Sonochem. 26 (2015) 361–369. doi:10.1016/j.ultsonch.2015.01.005.

[56] J. Lan, Y. Yang, X. Li, Microstructure and microhardness of SiC nanoparticles reinforced magnesium composites fabricated by ultrasonic method, Mater. Sci. Eng. A. 386 (2004) 284–290. doi:10.1016/j.msea.2004.07.024.

[57] W.S. Sarsam, A. Amiri, S.N. Kazi, A. Badarudin, Stability and thermophysical properties of non-covalently functionalized graphene nanoplatelets nanofluids, Energy Convers. Manag. 116 (2016) 101–111. doi:10.1016/j.enconman.2016.02.082.

[58] I.M. Mahbubul, T.H. Chong, S.S. Khaleduzzaman, I.M. Shahrul, R. Saidur, B.D. Long, M.A. Amalina, Effect of Ultrasonication Duration on Colloidal Structure and Viscosity of Alumina − Water Nanofluid, Ind. Eng. Chem. Res. 53 (2014) 6677–6684. doi:10.1021/ie500705.

[59] S. Marković, M. Mitrić, G. Starčević, D. Uskoković, Ultrasonic de-agglomeration of barium titanate powder, Ultrason. Sonochem. 15 (2008) 16–20. doi:10.1016/j.ultsonch.2007.07.008.

[60] F. Ali, L. Reinert, J.M. Levêque, L. Duclaux, F. Muller, S. Saeed, S.S. Shah, Effect of sonication conditions: Solvent, time, temperature and reactor type on the preparation of micron sized vermiculite particles, Ultrason. Sonochem. 21 (2014) 1002–1009. doi:10.1016/j.ultsonch.2013.10.010.

[61] B. Nickerson, Sample Preparation of Pharmaceutical Dosage Forms: Challanges and Strategies for Sample Preparation and Extraction, Springer, New York, 2011.

[62] K. Nogi, M. Naito, T. Yokoyama, eds., Nanoparticle technology handbook, Elsevier, 2012.

[63] C.-C. Li, S.-J. Chang, F.-J. Su, S.-W. Lin, Y.-C. Chou, Effects of capping agents on the dispersion of silver nanoparticles, Colloids Surfaces A Physicochem. Eng. Asp. 419 (2013) 209–215. doi:10.1016/j.colsurfa.2012.11.077.

[64] L.S. Wang, R.Y. Hong, Synthesis , Surface Modification and Characterisation of Nanoparticles, in: B. Reddy (Ed.), Adv. Nanocomposites - Synth. Charact. Ind. Appl., InTech, Rijeka, Croatia, 2011: pp. 289–322.

[65] S. Prakash, M.B. Karacor, S. Banerjee, Surface modification in microsystems and nanosystems, Surf. Sci. Rep. 64 (2009) 233–254. doi:10.1016/j.surfrep.2009.05.001.

[66] D. Qin, Z. Liu, H. Bai, D.D. Sun, X. Song, A new nano-engineered hierarchical membrane for concurrent removal of surfactant and oil from oil-in-water nanoemulsion, Sci. Rep. 6 (2016) 24365. doi:10.1038/srep24365.

[67] A. Asadi, M. Asadi, M. Siahmargoi, T. Asadi, M. Gholami Andarati, The effect of surfactant and sonication time on the stability and thermal conductivity of water-based nanofluid containing Mg(OH)2 nanoparticles: An experimental investigation, Int. J. Heat Mass Transf. 108 (2017) 191–198. doi:10.1016/j.ijheatmasstransfer.2016.12.022.

[68] F.S. Shariatmadar, S.G. Pakdehi, Effect of various surfactants on the stability time of

kerosene–boron nanofluids, Micro Nano Lett. 11 (2016) 498–502. doi:10.1049/mnl.2016.0223.

[69] M. Adil, H.M. Zaid, L.K. Chuan, N.R.A. Latiff, Effect of Dispersion Stability on Electrorheology of Water-Based ZnO Nanofluids, Energy and Fuels. 30 (2016) 6169–6177. doi:10.1021/acs.energyfuels.6b01116.

[70] Y.-S. Cho, G.-R. Yi, J.-J. Hong, S.H. Jang, S.-M. Yang, Colloidal indium tin oxide nanoparticles for transparent and conductive films, Thin Solid Films. 515 (2006) 1864–1871. doi:10.1016/j.tsf.2006.07.022.

[71] P. Tao, A. Viswanath, L.S. Schadler, B.C. Benicewicz, R.W. Siegel, Preparation and optical properties of indium tin oxide/epoxy nanocomposites with polyglycidyl methacrylate grafted nanoparticles, ACS Appl. Mater. Interfaces. 3 (2011) 3638–3645. doi:10.1021/am200841n.

[72] C.J. Capozzi, I.N. Ivanov, S. Joshi, and R.A. Gerhardt, The effect of atmopshere on optical properties of as-synthesized colloidal indium tin oxide colloidal, Nanotechnology. 20 (2009) 1–7. doi:10.1088/0957-4484/20/14/145701.

[73] R.A. Gilstrap, C.J. Capozzi, C.G. Carson, R.A. Gerhardt, C.J. Summers, Synthesis of a nonagglomerated indium tin oxide nanoparticle dispersion, Adv. Mater. 20 (2008) NA-NA. doi:10.1002/adma.200702556.

[74] J.S. Taurozzi, V.A. Hackley, M.R. Wiesner, Preparation of Nanoparticle Dispersions from Powdered Material Using Ultrasonic Disruption, NIST Spec. Publ. 1200-2. (2012) 1–10. doi:10.6028/NIST.SP.1200-2.

[75] D. V. Goia, E. Matijević, Preparation of monodispersed metal particles, New J. Chem. 22 (1998) 1203–1215. doi:10.1039/a709236i.

[76] E.N. Dattoli, W. Lu, ITO nanowires and nanoparticles for transparent films, MRS Bull. 36 (2011) 782–788. doi:10.1557/mrs.2011.212.

[77] G. Qin, L. Fan, A. Watanabe, Formation of indium tin oxide film by wet process using laser sintering, J. Mater. Process. Technol. 227 (2016) 16–23. doi:http://dx.doi.org/10.1016/j.jmatprotec.2015.07.011.

[78] Q. Zhang, H. Zhang, G. Xie, J. Zhang, Effect of surface treatment of magnetic particles on the preparation of magnetic polymer microspheres by miniemulsion polymerization, J. Magn. Magn. Mater. 311 (2007) 140–144. doi:10.1016/j.jmmm.2006.11.181.

[79] M. Cavazzuti, Optimization Methods: From Theory to Design, Modena, Italy, 2013. doi:10.1007/978-3-642-31187-1.

[80] C.F. Hwang, J.H. Chang, J.Y. Houng, C.C. Tsai, C.K. Lin, H.Y. Tsen, Optimization of medium composition for improving biomass production of Lactobacillus plantarum Pi06 using the Taguchi array design and the Box-Behnken method, Biotechnol. Bioprocess Eng. 17 (2012) 827–834. doi:10.1007/s12257-012-0007-4.

[81] D.C. Montgomery, Design and Analysis of Experiments, John Wiley & Sons, Danvers, 2012. doi:10.1198/tech.2006.s372.

[82] K.A. Huynh, K.L. Chen, Aggregation kinetics of citrate and polyvinylpyrrolidone coated silver nanoparticles in monovalent and divalent electrolyte solutions, Environ. Sci. Technol. 45 (2011) 5564–5571. doi:10.1021/es200157h.

[83] K.L. Chen, M. Elimelech, Aggregation and deposition kinetics of fullerene (C60) nanoparticles, Langmuir. 22 (2006) 10994–11001. doi:10.1021/la062072v.

[84] T. Mohammadi, A. Moheb, M. Sadrezadeh, A. Razmi, Separation of copper ions by electrodialysis using Taguchi experimental design, Desalination. 169 (2004) 21–31. doi:10.1016/j.

[85] M. Sadrzadeh, A. Razmi, T. Mohammadi, Separation of different ions from wastewater at various operating conditions using electrodialysis, Sep. Purif. Technol. 54 (2007) 147–156. doi:10.1016/j.seppur.2006.08.023.

[86] E. Saljoughi, M. Sadrzadeh, T. Mohammadi, Effect of preparation variables on morphology and pure water permeation flux through asymmetric cellulose acetate membranes, J. Memb. Sci. 326 (2009) 627–634.

[87] J. Singh, R. Singh, H. Singh, Repeatability of linear and radial dimension of ABS replicas fabricated by fused deposition modelling and chemical vapor smoothing process: A case study, Meas. J. Int. Meas. Confed. 94 (2016) 5–11. doi:10.1016/j.measurement.2016.07.064.

[88] B. Khorshidi, T. Thundat, D. Pernitsky, M. Sadrzadeh, A parametric study on the synergistic impacts of chemical additives on permeation properties of thin film composite polyamide membrane, J. Memb. Sci. 535 (2017) 248–257. doi:10.1016/j.memsci.2017.04.052.

[89] B. Khorshidi, T. Thundat, B.A. Fleck, M. Sadrzadeh, Thin film composite polyamide

membranes: parametric study on the influence of synthesis conditions, RSC Adv. 5 (2015) 54985–54997. doi:10.1039/C5RA08317F.

[90] R.K. Roy, A primer on the Taguchi method, Second Edi, Society of Manfacturing Engineering, 2010.

[91] R.K. Roy, Design of Experiments Using The Taguchi Approach: 16 Steps to Product and Process Improvement, John Wiley & Sons, Inc., 2001.

[92] T. Meißner, K. Oelschlägel, A. Potthoff, Dispersion of nanomaterials used in toxicological studies: A comparison of sonication approaches demonstrated on TiO2 P25, J. Nanoparticle Res. 16 (2014). doi:10.1007/s11051-013-2228-7.

[93] S. Horikoshi, N. Serpone, Introduction to Nanoparticles, in: Microwaves Nanoparticle Synth. Fundam. Appl., 1st ed., Wiley-VCH Verlag GmbH & Co. KGaA, 2013: pp. 1–24. doi:10.1002/9783527648122.ch1.

[94] B.I. Kharisov, H.V.R. Dias, O. V. Kharissova, A. Vázquez, Y. Peña, I. Gómez, Solubilization, dispersion and stabilization of magnetic nanoparticles in water and non-aqueous solvents: recent trends, RSC Adv. 4 (2014) 45354–45381. doi:10.1039/C4RA06902A.

[95] E. Engineering, E.H. Sciences, L. Angeles, Dispersion and Stability Optimization of TiO2 Nanoparticles in Cell Culture Media, Environ. Sci. Technol. 44 (2010) 7309–7314.

[96] Y.S. Cho, H.M. Kim, J.J. Hong, G.R. Yi, S.H. Jang, S.M. Yang, Dispersion stabilization of conductive transparent oxide nanoparticles, Colloids Surfaces A Physicochem. Eng. Asp. 336 (2009) 88–98. doi:10.1016/j.colsurfa.2008.11.014.

[97] Q. Xu, Z. Lei, Y. Yao, Dispersion stability of indium tin oxide nanoparticles in butyl acetate, in: 2011 Int. Conf. Remote Sensing, Environ. Transp. Eng., IEEE, Nanjing, China, 2011: pp. 5876–5879.

[98] A.P. Lagrow, B. Ingham, M.F. Toney, R.D. Tilley, Effect of Surfactant Concentration and Aggregation on the Growth Kinetics of Nickel Nanoparticles, J. Phys. Chem. C. 117 (2013) 16709−16718.

[99] D.H. Napper, Steric stabilization, J. Colloid Interface Sci. 58 (1977) 390–407. doi:10.1016/0021-9797(77)90150-3.

[100] A.W. Pacek, P. Ding, A.T. Utomo, Effect of energy density, pH and temperature on de-aggregation in nano-particles/water suspensions in high shear mixer, Powder Technol. 173

(2007) 203–210. doi:10.1016/j.powtec.2007.01.006.

[101] A. Kumar, T. Kumaresan, A.B. Pandit, J.B. Joshi, Characterization of flow phenomena induced by ultrasonic horn, Chem. Eng. Sci. 61 (2006) 7410–7420. doi:10.1016/j.ces.2006.08.038.

[102] N. Gondrexon, V. Renaudin, C. Petrier, M. Clement, P. Boldo, Y. Gonthier, A. Bernis, Experimental study of the hydrodynamic behaviour of a high frequency ultrasonic reactor., Ultrason. Sonochem. 5 (1998) 1–6. doi:10.1016/S1350-4177(97)00043-6.

[103] M. Chouvellon, A. Largillier, T. Fournel, P. Boldo, Y. Gonthier, Velocity study in an ultrasonic reactor, Ultrason. Sonochem. 7 (2000) 207–211. doi:10.1016/S1350-4177(00)00060-2.

[104] V. Frenkel, R. Gurka, A. Liberzon, U. Shavit, E. Kimmel, Preliminary investigations of ultrasound induced acoustic streaming using particle image velocimetry, Ultrasonics. 39 (2001) 153–156. doi:10.1016/S0041-624X(00)00064-0.

[105] L. Ma, F. Chen, G. Shu, Preparation of fine particulate reinforced metal matrix composites by high intensity ultrasonic treatment, J. Mater. Sci. Lett. 14 (1995) 649–650.

[106] C. Sauter, M.A. Emin, H.P. Schuchmann, S. Tavman, Influence of hydrostatic pressure and sound amplitude on the ultrasound induced dispersion and de-agglomeration of nanoparticles, Ultrason. Sonochem. 15 (2008) 517–523. doi:10.1016/j.ultsonch.2007.08.010.

[107] S.H. Chu, S.H. Choi, J.W. Kim, G.C. King, J.R. Elliott, Ultrasonication of bismuth telluride nanocrystals fabricated by solvothermal method, in: SPIE 13th Annu. Int. Symp. Smart Struct. Mater., NASA Technical Reports Server, San Diego, CA, USA, 2006: pp. 1–8. doi:10.1117/12.658071.

[108] R.S. Davidson, A. Safdar, J.D. Spencer, B. Robinson, Applications of ultrasound to organic chemistry, Ultrasonics. 25 (1987) 35–39. doi:10.1016/0041-624X(87)90009-6.

[109] K.S. Suslick, S.J. Doktycz, E.B. Flint, On the origin of sonoluminescence and sonochemistry, Ultrasonics. 28 (1990) 280–290. doi:10.1016/0041-624X(90)90033-K.

[110] T. Prozorov, R. Prozorov, K.S. Suslick, High velocity interparticle collisions driven by ultrasound, J. Am. Chem. Soc. 126 (2004) 13890–13891. doi:10.1021/ja049493o.

[111] S.J. Doktycz, K.S. Suslick, Interparticle collisions driven by ultrasound, Science (80-.). 247 (1990) 1067–1069. doi:10.1126/science.2309118.

[112] S.R. Raine, H.B. So, An Investigation of the relationships between dispersion, power, and mechanical energy using the end-over-end shaking and ultrasonic methods of aggregate stability assessment, Aust. J. Soil Res. 35 (1997) 41–53. doi:10.1071/SR99114.

[113] B. Khorshidi, A. Bhinder, T. Thundat, D. Pernitsky, M. Sadrzadeh, Developing high throughput thin film composite polyamide membranes for forward osmosis treatment of SAGD produced water, J. Memb. Sci. 511 (2016) 29–39. doi:10.1016/j.memsci.2016.03.052.

[114] J. Lee, H.R. Chae, Y.J. Won, K. Lee, C.H. Lee, H.H. Lee, I.C. Kim, J. min Lee, Graphene oxide nanoplatelets composite membrane with hydrophilic and antifouling properties for wastewater treatment, J. Memb. Sci. 448 (2013) 223–230. doi:10.1016/j.memsci.2013.08.017.

[115] Z. Almansoori, B. Khorshidi, B. Sadri, M. Sadrzadeh, Parametric study on the stabilization of metal oxide nanoparticles in organic solvents: A case study with indium tin oxide (ITO) and heptane, Ultrason. Sonochem. 40 (2017) 1003–1013. doi:10.1016/j.ultsonch.2017.09.012.

[116] J.F. Li, Z.L. Xu, H. Yang, L.Y. Yu, M. Liu, Effect of TiO2 nanoparticles on the surface morphology and performance of microporous PES membrane, Appl. Surf. Sci. 255 (2009) 4725–4732. doi:10.1016/j.apsusc.2008.07.139.

[117] B. Khorshidi, T. Thundat, B.A. Fleck, M. Sadrzadeh, Thin film composite polyamide membranes: parametric study on the influence of synthesis conditions, RSC Adv. 5 (2015) 54985–54997. doi:10.1039/C5RA08317F.

[118] J. María Arsuaga, A. Sotto, G. del Rosario, A. Martínez, S. Molina, S.B. Teli, J. de Abajo, Influence of the type, size, and distribution of metal oxide particles on the properties of nanocomposite ultrafiltration membranes, J. Memb. Sci. 428 (2013) 131–141. doi:10.1016/j.memsci.2012.11.008.

[119] W.J. Lau, A.F. Ismail, P.S. Goh, N. Hilal, B.S. Ooi, Characterization methods of thin film composite nanofiltration membranes, Sep. Purif. Rev. 44 (2015) 135–156. doi:10.1080/15422119.2014.882355.

[120] K.L. Tu, A.R. Chivas, L.D. Nghiem, Effects of membrane fouling and scaling on boron rejection by nanofiltration and reverse osmosis membranes, Desalination. 279 (2011) 269–277. doi:10.1016/j.desal.2011.06.019.

[121] A. Resosudarmo, Y. Ye, P. Le-Clech, V. Chen, Analysis of UF membrane fouling mechanisms caused by organic interactions in seawater, Water Res. 47 (2013) 911–921. doi:10.1016/j.watres.2012.11.024.

[122] R. Zhang, W. Shi, S. Yu, W. Wang, Z. Zhang, B. Zhang, L. Li, X. Bao, Influence of salts, anion polyacrylamide and crude oil on nanofiltration membrane fouling during desalination process of polymer flooding produced water, Desalination. 373 (2015) 27–37. doi:10.1016/j.desal.2015.07.006.

[123] L.O. Villacorte, Y. Ekowati, H. Winters, G. Amy, J.C. Schippers, M.D. Kennedy, MF/UF rejection and fouling potential of algal organic matter from bloom-forming marine and freshwater algae, Desalination. 367 (2015) 1–10. doi:10.1016/j.desal.2015.03.027.

[124] S. Jeong, L.H. Kim, S.J. Kim, T.V. Nguyen, S. Vigneswaran, I.S. Kim, Biofouling potential reductions using a membrane hybrid system as a pre-treatment to seawater reverse osmosis, Appl. Biochem. Biotechnol. 167 (2012) 1716–1727. doi:10.1007/s12010-011-9514-6.

[125] R.J. Wakeman, E.S. Tarleton, Membrane fouling prevention in crossflow microfiltration by the use of electric fields, Chem. Eng. Sci. 42 (1987) 829–842. doi:10.1016/0009-2509(87)80042-8.

[126] H.M. Huotari, G. Trägårdh, I.H. Huisman, Crossflow Membrane Filtration Enhanced by an External DC Electric Field: A Review, Chem. Eng. Res. Des. 77 (1999) 461–468. doi:10.1205/026387699526304.

[127] S. Bayar, A. Karagunduz, B. Keskinler, Influences of electroosmosis and electrophoresis on permeate flux and membrane fouling in submerged membrane bioreactors (SMBRs), Water Sci. Technol. 74 (2016) 766–776. doi:10.2166/wst.2016.280.

[128] J. Huang, Z. Wang, J. Zhang, X. Zhang, J. Ma, Z. Wu, A novel composite conductive microfiltration membrane and its anti-fouling performance with an external electric field in membrane bioreactors, Sci Rep. 5 (2015) 9268. doi:10.1038/srep09268.

[129] B. Jiang, C. Du, S. Shi, L. Tan, M. Li, J. Liu, L. Xue, X. Ji, Enhanced treatment performance of coking wastewater and reduced membrane fouling using a novel EMBR, Bioresour. Technol. 229 (2017) 39–45. doi:10.1016/j.biortech.2016.12.116.

[130] D. Stillman, L. Krupp, Y.H. La, Mesh-reinforced thin film composite membranes for forward osmosis applications: The structure-performance relationship, J. Memb. Sci. 468

(2014) 308–316. doi:10.1016/j.memsci.2014.06.015.

[131] X. Liu, S.L. Ong, H.Y. Ng, Fabrication of mesh-embedded double-skinned substrate membrane and enhancement of its surface hydrophilicity to improve anti-fouling performance of resultant thin-film composite forward osmosis membrane, J. Memb. Sci. 511 (2016) 40–53. doi:10.1016/j.memsci.2016.03.015.